

Contents lists available at ScienceDirect

Biomaterials

journal homepage: www.elsevier.com/locate/biomaterials





Sequential activation of heterogeneous macrophage phenotypes is essential for biomaterials-induced bone regeneration

Wei Qiao a,b,1 , Huizhi Xie a,b,1 , Jinghan Fang a,b,1 , Jie Shen a,b , Wenting Li c , Danni Shen c , Jun Wu b , Shuilin Wu d , Xuanyong Liu e,f , Yufeng Zheng c , Kenneth M.C. Cheung a,b , Kelvin W. K. Yeung a,b,f,*

- a Department of Orthopaedics & Traumatology, Li Ka Shing Faculty of Medicine, The University of Hong Kong, Pokfulam, Hong Kong, 999077, China
- ^b Shenzhen Key Laboratory for Innovative Technology in Orthopaedic Trauma, Department of Orthopaedics and Traumatology, The University of Hong Kong-Shenzhen Hospital, Shenzhen, 518053, China
- ^c State Key Laboratory for Turbulence and Complex System and Department of Materials Science and Engineering, College of Engineering, Peking University, Beijing, 100871. PR China
- d School of Materials Science and Engineering, the Key Laboratory of Advanced Ceramics and Machining Technology by the Ministry of Education of China, Tianjin University, Tianjin, 300072, China
- e State Key Laboratory of High Performance Ceramics and Superfine Microstructure, Shanghai Institute of Ceramics, Chinese Academy of Sciences, Shanghai, PR China
- f Cixi Center of Biomaterials Surface Engineering, Shanghai Institute of Ceramics, Chinese Academy of Sciences, Ningbo, PR China

ARTICLE INFO

Keywords: Macrophage Bone regeneration Osteogenesis Angiogenesis Immunomodulation

ABSTRACT

Macrophage has been gradually recognized as a central regulator in tissue regeneration, and the study of how macrophage mediates biomaterials-induced bone regeneration through immunomodulatory pathway becomes popular. However, the current understanding on the roles of different macrophage phenotypes in regulating bone tissue regeneration remains controversial. In this study, we demonstrate that sequential infiltration of heterogeneous phenotypes of macrophages triggered by bio-metal ions effectively facilitates bone healing in bone defect. Indeed, M1 macrophages promote the recruitment and early commitment of osteogenic and angiogenic progenitors, while M2 macrophages and osteoclasts support the deposition and mineralization of the bone matrix, as well as the maturation of blood vessels. Moreover, we have identified a group of bone biomaterial-related multinucleated cells that behave similarly to M2 macrophages with wound-healing features rather than participate in the bone resorption cascade similarly to osteoclasts. Our study shows how sequential activation of macrophage-osteoclast lineage contribute to a highly orchestrated immune response in the bone tissue microenvironment around biomaterials to regulate the complex biological process of bone healing. Therefore, we believe that the temporal activation pattern of heterogeneous macrophage phenotypes should be considered when the next generation of biomaterials for bone regeneration is engineered.

1. Introduction

The skeletal system has been known for its potential to restore damaged tissue to its pre-injury cellular composition, structure, and biomechanical function. However, the involved biological processes are complicated and long-lasting [1]. Over the decades, a number of osteogenic factors have been introduced to bone biomaterials to accelerate bone tissue repair; however, it remains quite challenging to sustain the quantity and quality of peak bone mass after the completion of bone

repair [2]. Thus, there is an urgent need for novel bone biomaterials that could actively interact with the different effector cells involved in the biological events during bone regeneration to better take advantage of the natural bone-healing process. In recent years, with the rapid advancement in osteoimmunology, there has been a paradigm shift from the conventional biomaterials with osteopromotive potential to the biomaterials with immunomodulatory effects [3]. This concept emphasizes the central roles of the immune response in coordinating biomaterials' interaction with the bone tissue microenvironment that

^{*} Corresponding author. Department of Orthopaedics & Traumatology, Li Ka Shing Faculty of Medicine, The University of Hong Kong, Pokfulam, Hong Kong, 999077, China.

E-mail address: wkkyeung@hku.hk (K.W.K. Yeung).

¹ Equal contributions.

subsequently regulates the cellular functions of osteogenic and angiogenic progenitors during the regeneration course [3].

Owing to the central role of macrophages in the immune reaction to bone biomaterials, as well as their heterogeneity and plasticity, macrophages have been recognized as the major target cells for immunomodulation in the biomaterial field [4]. It is now generally believed that the macrophages involved in healing bone injury are primarily derived from the resident population of macrophages in bone tissue, namely OsteoMacs [2]. This subset of the CD68⁺ cell type constitutes approximately one-sixth of all cells residing in the bone marrow and extensively covers the bone surface with a stellate morphology [5]. Moreover, they are demonstrated to be closely associated with in situ bone modeling by forming a distinctive canopy structure covering more than 75% of osteoblasts throughout their life span [5]. In addition to their well-known ability to detect bone damage and recruit other cells to initiate the bone-remodeling process [6], it is becoming evident that besides the early acute immune response, macrophages are actively engaged in almost every phase of the bone-healing process [2,5]. These findings imply that macrophages serve as an integral component of bone tissue to survey the alteration in the bone microenvironment, as well as mediate bone homeostasis upon injury.

Macrophages exist on a spectrum of phenotypes, ranging from the "classically activated" M1 macrophages, which are known for their production of pro-inflammatory cytokines, to the "alternatively activated" M2 macrophages, which secrete anti-inflammatory factors [7]. While M1 macrophages are indispensable for the initiation of the regeneration process, M2 macrophages are reported to be more prevalent in the late bone-modeling/remodeling stage [8]. Therefore, the heterogeneous population of macrophages appears to be accurately positioned and transcriptionally programmed to play different but complementary roles through the whole cascade of bone healing. However, the current understanding on how these two phenotypes of macrophages coordinate their cellular functions in bone tissue regeneration upon the stimulation of implanted biomaterials has yet to be clarified. Based on the observation that the prolonged pro-inflammatory phase might delay the bone-healing process [9], many researchers have developed their bone biomaterials that solely promote M2 macrophages but inhibit M1 macrophages [3]. However, we believe that a properly balanced population of M1 and M2 throughout the bone-healing process is essential for achieving effective and efficient bone tissue regeneration.

Macrophages appear to process a particularly pronounced potential to fuse among themselves, under both physiological and pathological conditions [10]. An intriguing cell type originating from macrophages, namely multinucleated giant cells (MNGCs), is commonly observed during bone regeneration, especially when osteogenic biomaterials are implanted [4]. These MNGCs were suggested to primarily facilitate the uptake of large particles, since interleukin (IL)-4-induced MNGCs were reported to phagocytose large and complement-opsonized materials more effectively than their unfused precursors [11]. However, other long-term studies reported that the MNGCs were barely capable of degrading biomaterials, i.e., calcium phosphate-based bone substitutes, even after implanted for 14-80 months [12,13]. Despite the understanding on the cellular behaviors and functions of MNGCs in response to pathogens [14] and soft tissue biomaterials [15], the knowledge gained seems inapplicable to the MNGCs observed around biomaterials during bone regeneration. Compared with the MNGCs, the osteoclast is another kind of more well-defined macrophage-derived multinucleated cells frequently observed around bone biomaterials. While the mononuclear osteoclast progenitor can be found on or near the bone surface, the fusion of mature osteoclasts primarily occurs on the bone surface [16]. Apart from their primary bone resorptive function, osteoclasts have been known to participate in bone formation through the intertwined coupling with osteoblasts during the bone-modeling and remodeling process [17]. Over the past few years, increasing evidence has indicated that the presence of tartrate-resistant acid phosphatase (TRAP) positive cells at the early stage of bone healing would favor new

bone formation by modulating the osteoblast and angiogenic activities [18–21]. Therefore, we believe that the significance of osteoclasts around bone biomaterials for new bone formation has long been underestimated.

Therefore, our study aims at unveiling the central role of the macrophage-osteoclast lineage in regulating bone regeneration based on our established works using bio-metal ions to induce osteogenesis [22-28]. We systematically characterized the sequential activation pattern of heterogeneous macrophage phenotypes during the bone-healing process and tested our hypothesis using Mg²⁺-releasing alginate hydrogel in a rat femoral defect model. Moreover, we provided a side-by-side comparison in vitro to address the immunomodulatory effects of several identical macrophage phenotypes on osteogenesis and angiogenesis with a carefully designed coculture system using primary bone marrow-derived macrophages (BMMs), mesenchymal stem cells (MSCs), and endothelial cells (ECs). Our findings demonstrate how a highly immune response mediated by orchestrated cyte-macrophage-osteoclast lineage contributes to the recruitment and commitment of osteogenic and vascular progenitor cells in the bone tissue regenerative process in the interplay with osteogenic

2. Materials and methods

2.1. Animal studies

2.1.1. Animal surgery

All the animal procedures were performed in accordance with a protocol approved by the Committee on the Use of Live Animals in Teaching and Research (CULATR, the University of Hong Kong). In brief, twenty 6-8-week-old female Sprague Dawley (SD) rats, weighing 200-250 g, were purchased from Charles River Laboratories (USA) and maintained in a specific pathogen-free facility (Centre for Comparative Medicine Research, CCMR, HKU). Before the operation, each rat was anesthetized via intraperitoneal injections of ketamine hydrochloride (67 mg/kg; Alfamine, Alfasan International B.V., Holland) and xylazine hydrochloride (6 mg/kg; Alfazyne, Alfasan International B.V., Holland). A 2-mm-diameter tunnel defect was prepared at the lateral epicondyle of the left femur using a hand driller. After a thorough irrigation using saline, - Mg²⁺-releasing alginate was injected into the defect. In the control group, pure alginate was injected. After the surgical wound was closed with suture, the rats immediately received subcutaneous injections of terramycin (1 mg/kg) and ketoprofen (0.5 mg/kg). For the depletion of phagocytic macrophage, liposomal clodronate (0.5 mg/kg) was administered weekly via intraperitoneal injection, starting 1 week prior to the bone injury.

2.1.2. Histological analysis

After being sacrificed at the designated time points (i.e, day 3, 7, 14, 56) by overdose intraperitoneal injection of pentobarbital, the femora were dislocated and fixed in 4% paraformaldehyde solution for 24 h. The samples were then decalcified with 12.5% ethylenediaminetetraacetic acid (EDTA, Sigma-Aldrich, USA) for 6 weeks, being dehydrated through a series of graded ethanol and embedded in paraffin. The specimens were cut into 5-µm-thick sections using a rotary microtome (RM215, Leica Microsystems, Germany). Masson's trichrome (Solarbio, China) staining, hematoxylin and eosin (H&E, Sigma-Aldrich, USA) staining, and TRAP (Sigma-Aldrich, USA) staining were performed on selected sections from each sample, following the manufacturer's instructions. Histological images were captured using the Vectra Polaris Imaging System (Akoya Biosciences, USA).

2.1.3. Micro-CT (µCT) analysis

To monitor the healing process and examine the new bone formation in the defect, the femoral defect was scanned by a live animal μCT scanning device (SkyScan 1076, Kontich, Belgium) at serial time points

after the operation (i.e., 0, 3, 7, 14, 28, and 56 days). The scanning procedure used an 88-kV voltage with a 100- μ A current. The resolution was set at 17.3 μ m/pixel. Two calibration phantom rods with standard densities of 0.25 and 0.75 g/cm³ were scanned with each rat. The μ CT data were reconstructed using the NRecon software (Skyscan Company), the bone mineral density (BMD) heat mapping was reconstructed using the CTvox software (Skyscan Company), and the image processing and analysis were performed using the CTAn software (Skyscan Company).

2.1.4. Immunohistochemistry (IHC) analysis

The dewaxed slides were treated with Proteinase K (Sigma-Aldrich, USA) for proteolytic digestion and with $3\%~H_2O_2$ for the elimination of endogenous peroxidase activity. After a 1-h blocking with normal goat serum, the slides were incubated with specific primary antibodies overnight at 4 °C. The primary antibodies used in this study included mouse anti-CD68 (Abcam, USA), rabbit anti-CD206 (Abcam, USA), and rabbit anti-iNOS (Abcam, USA). The slides were then incubated with Alexa-Fluor 488 conjugated anti-rabbit IgG or Alexa-Fluor 647 conjugated anti-mouse IgG secondary antibodies (ThermoFisher, USA) and Hoechst 33324 (ThermoFisher, USA). Immunofluorescent images were captured using an LSM 780 confocal microscopy (Zeiss, Germany).

2.1.5. Multiplex IHC analysis

Antigen retrieval and blocking were performed on the dewaxed slides using the Antigen retrieval reagent (pH 6.0) and Blocking/antibody diluent provided in the Opal Polaris Multicolor Manual IHC Detection Kit (Akoya Biosciences, USA), following the manufacturer's instructions. In brief, the incubation of each primary antibody was done overnight at 4 °C. The primary antibodies used in this study included rabbit anti-CD68 (Abcam, USA), mouse anti-TRAP (Abcam), rabbit anti-CD206 (Abcam, USA), rabbit anti-iNOS (Abcam, USA), and rabbit anti-Osterix (Abcam, USA). Between each incubation of the primary antibody, tyramide signal amplification (TSA) visualization was performed using the Opal Polymer Horseradish peroxidase (HRP) secondary antibody and fluorophores: Opal 520, Opal 570, Opal 620, Opal 690, and DAPI (Akoya Biosciences, USA). The stained slides were imaged using the Vectra Polaris Imaging System (Akoya Biosciences, USA).

2.2. Cell culture studies

2.2.1. Cell isolation and treatment

For the isolation of endothelial cells (ECs), mesenchymal stem cells (MSCs), and bone marrow macrophages (BMMs), 8-week-old C57L6/J mice were euthanized with a dosage of intraperitoneal injection of Pentobarbital. The ECs were isolated from the mouse aorta, as previously described elsewhere [29]. In brief, after the exposure of abdomen, 1 mL 1000 U/mL of heparin was directly injected into the left ventricle to prevent blood coagulation, while the abdominal aorta was cut to release the blood. The aorta was dissected and immersed in ice-cold 1x phosphate-buffered saline (PBS). The aorta segment was then cut into 1-mm pieces and flattened to be attached to the 0.1% gelatin-coated plates with the lumen side facing down. After 3-5 days, when ECs would sprout out of the tissue, the tissue could be removed. The isolated ECs were cultured in 0.1% gelatin (Sigma-Aldrich, USA)-coated flasks in a Dulbecco's Modified Eagle Medium/Nutrient Mixture F-12 (DMEM/F12) medium (Gibco, USA), supplemented with 10% fetal bovine serum (FBS, Gibco, USA) and 1% Penicillin-Streptomycin (Gibco, USA). The culture medium was refreshed every 2 days, and only passages 3-5 were used for the experiments. MSCs and BMMs were isolated from the femora and the tibiae. Briefly, the soft tissues attached to the dislocated femora and tibiae were carefully removed using forceps and gauze; the long bones were cut into pieces before vigorous resuspension of whole bone marrow cells in a serum-free DMEM medium (Gibco, USA) using a vortex mixer. The bone chips and debridement were removed by passing the mixture through a cell strainer. After centrifugation, the cell pellet was resuspended in a DMEM medium,

supplemented with 10% FBS and 1% Penicillin-Streptomycin (complete DMEM medium), and cultured in culture flasks. After a 6-h incubation in a humidified incubator with 5% $\rm CO_2$ at 37 °C, the unattached cells were gently removed for the induction of BMMs. Meanwhile, the attached bone marrow cells were gently washed in PBS and further cultured as MSCs in a complete DMEM medium until they reached 80% confluence. The culture medium was refreshed every 2 days, and only passages 3–5 were used for the experiments. To verify the purity of MSCs, we used a mouse mesenchymal stem cell multi-color flow kit (R&D, USA) to quantify the percentage of CD29+, Sca-1+, and CD45-cells using a flow cytometer (NovoCyte Quanteon, ACEA Biosciences, USA) according to the manufacturer's instruction.

After the 6-day macrophage induction using a complete DMEM medium supplemented with 20 ng/ml of macrophage colonystimulating factor (M-CSF), the BMMs became adherent, and the culture medium was replaced by a different polarization medium. For M1like macrophage differentiation, the complete DMEM was supplemented with 10 ng/ml of interferon-gamma (IFN-y, R&D System, USA) and 10 ng/ml of lipopolysaccharide (LPS, R&D System, USA). For M2-like macrophage differentiation, the complete DMEM was supplemented with 10 ng/ml of IL-4 (R&D System, USA) and 10 ng/ml of IL-13 (R&D System, USA). For the preosteoclast (pOC) differentiation, the complete DMEM was supplemented with 50 ng/ml of receptor activator of nuclear factor kappa-B ligand (RANKL, R&D System, USA) and 20 ng/ml of M-CSF (R&D System, USA). The BMMs cultured in a complete DMEM medium served as a control (M0-like). After the 6-day polarization, the induction medium was replaced by a fresh complete DMEM medium for another 24-h incubation. The supernatant was then collected, centrifuged, and filtered with 0.22-µm filters (Millipore, USA) before storage at $-80\,^{\circ}\text{C}$. The conditioned medium for the indirect coculture of MSCs and ECs (Fig. 4a) was prepared by mixing the supernatant from the polarized BMMs with a fresh complete DMEM medium at a ratio of 1:1

2.2.2. Real-time quantitative polymerase chain reaction (RT-qPCR) assay The total RNA of the cells (i.e., BMMs, MSCs, and ECs) was extracted and purified using an RNeasy Plus kit (Qiagen, USA), following the manufacturer's instructions. For the reverse transcript, complementary DNA was synthesized using a Takara RT Master Mix (Takara, Japan), following the manufacturer's instructions. The primers used in the RT-qPCR assay were synthesized using Integrated DNA Technologies (IDT, Singapore), based on sequences retrieved from the Primer Bank (http://pga.mgh.harvard.edu/primerbank/, Table S1). The SYBR Green Premix Ex Taq (Takara, Japan) was used for the amplification and detection of cDNA targets on the LightCycler480 Real-time PCR system (Roche, USA). The mean cycle threshold (Ct) value of each target gene was normalized to the housekeeping gene GAPDH. The results were shown in a fold change using the ΔΔCt method.

2.2.3. Western blotting

After the treatment, the BMMs were rinsed with ice-cold PBS and lysed with the RIPA Lysis and Extraction Buffer (ThermoFisher, USA) containing 1% Phosphatase Inhibitor Cocktail (ThermoFisher, USA). After centrifugation at 15,000×g for 10 min at 4 °C, the supernatants were collected to measure the protein concentration using the BCA Protein Assay Kit (ThermoFisher, USA). A total of 25 μg of protein from each sample was subjected to sodium dodecyl sulfate polyacrylamide gel electrophoresis (SDS-PAGE) and transferred to the polyvinylidene difluoride (PVDF) membrane (Merck Millipore, USA). Then, the membrane was blocked in 5% w/v bovine serum albumin (BSA, Sigma-Aldrich, USA) and incubated with blocking buffer-diluted primary antibodies overnight at 4 °C. The primary antibodies used included mouse anti-NFATc1 (Santa Cruz, USA), rabbit anti-Integrin β1 (CST, USA), rabbit anti-Phospho-FAK (CST, USA), rabbit anti-FAK (CST, USA), rabbit anti-GAPDH (CST, USA). The protein bands were visualized by using conjugated secondary antibodies and an enhanced

chemiluminescence (ECL) substrate (Advansta, USA) and exposed under the Typhoon5 Biomolecular Imager 680 (GE Amersham, USA).

2.2.4. Immunocytochemistry analysis

Following the polarization in the induction medium, the cultured BMMs were washed with 1x PBS three times, fixed with 4% paraformaldehyde after permeabilization with 0.2% Triton X-100 for 10 min. The primary antibodies used included anti-NF-κB p65 (CST, USA), mouse anti-NFATc1 (Santa Cruz, USA), rabbit anti-CD68 (Abcam, USA), and rabbit anti-CD206 (Abcam, USA). The secondary antibodies used included Alexa-Fluor 488 conjugated anti-rabbit IgG (ThermoFisher, USA) and Alexa-Fluor 647 conjugated anti-mouse IgG (ThermoFisher, USA). Rhodamine Phalloidin (Sigma-Aldrich, USA) and Hoechst 33342 (ThermoFisher, USA) were used for counterstaining. The fluorescent images were captured using an LSM 980 confocal microscope (Carl Zeiss, Germany). The expression of NFATc1 or CD206 was quantified by the fluorescent intensity in either 647 nm channel or 488 nm channel using ImageJ software (NIH, USA). The results were presented as fold change in the fluorescent intensity by comparing the tested group to the control group.

2.2.5. Cytokine array

The cytokines and chemokines produced by BMMs after the polarization in different induction mediums were tested using a Proteome Profiler antibody array (R&D System, USA), following the manufacturer's instructions. The supernatants from the BMMs were incubated with the nitrocellulose membranes overnight after the addition of the mouse cytokine array detection antibody cocktail. Next, the membranes were thoroughly washed in a 1x wash buffer in a rocking platform shaker and incubated with Streptavidin-HRP for 30 min. The signals were visualized by using a Chemi Reagent Mix under a Typhoon5 Biomolecular Imager 680 (GE Amersham, USA).

2.2.6. Cell proliferation assay

The proliferation of the MSCs and ECs cultured in a conditioned medium was assessed by measuring the cell viability using a cell counting kit-8 (CCK-8, Dojindo, Japan). The MSCs and ECs were seeded in 96-well plates at a density of $1\times10^4/\text{cm}^2$ and treated with a BMM-derived conditioned medium. On Day 3 and Day 7 after the stimulation, the culture medium was replaced with 100 μl of fresh serum-free DMEM, supplemented with 10 μl of CCK-8 reagent. After a 2-h incubation, the absorbance at 450 nm was detected by a Multiskan GO microplate reader (ThermoFisher, USA). The cell viability was presented as a percentage by comparing the optical density (OD) value of the tested group with that of the control group (M0 conditioned medium treated group).

2.2.7. Wound-healing assay

The migration of the MSCs and ECs cultured in a conditioned medium was assessed by a wound-healing assay. The MSCs and ECs were seeded in 24-well plates at a density of $5\times10^4/\text{cm}^2$ and cultured overnight for attachment. A scratch was created in each well using a 200-µl tip. The cells were washed with PBS to remove the cell debris and then treated using different BMM-derived conditioned mediums. For wound healing of ECs, the microscopic images of the same view were taken at 0h, 6 h, 12 h, and 24 h, while for MSCs, the microscopic images of the same view were taken at 0h,24 h, 48 h, and 72 h. The wound area was measured by the ImageJ software (NIH, USA), and the wound closure rate was calculated by dividing the reduction in the wound area at a designated time point by the wound area at the initial time point.

2.2.8. Transwell migration assay

The migration of the MSCs stimulated by the conditioned medium was assessed by a transwell migration assay. After overnight starving in serum-free culture medium, the MSCs were seeded in the 96-well transwell inserts at a density of $3.6 \times 10^4/\text{cm}^2$. Meanwhile, the

conditioned medium harvested from various phenotypes of BMMS was supplemented with fresh DMEM containing 30% FBS and added into the lower chambers. After 24 h incubation to allow the migration of MSCs to the lower side of the membrane, the inserts were removed from the plate and fixed using 4% PFA. The non-migrated cells in the inserts were removed by cotton swab, whereas the migrated cells were stained with 0.5% crystal violet (Sigma-Aldrich, USA). The images of the migrated MSCs were captured using a Leica DM IL LED microscope (Carl Zeiss, Germany) and the number of migrated cells was quantified manually using the ImageJ software (NIH, USA).

2.2.9. Alkaline phosphatase (ALP) staining

The osteogenic activity of the MSCs cultured in a conditioned medium was assessed by ALP staining. The MSCs were seeded in 96-well plates at a density of $1\times10^4/\mathrm{cm}^2$ and treated with BMM-derived conditioned medium. On Day 3 and Day 7 after the stimulation, the cells were fixed with 4% paraformaldehyde for 10 min. After the cells were thoroughly washed with PBS, they were incubated with the 1-Step NBT/BCIP substrate solution (ThermoFisher, USA) for 15 min in the dark. The images were captured under a Leica DM IL LED microscope (Carl Zeiss, Germany), and the number of ALP positive cells was quantified manually using the ImageJ software (NIH, USA).

2.2.10. Tube formation assay

The angiogenic activity of the ECs cultured in a conditioned medium was assessed by tube formation assay. The 96-well plates were coated with the Matrigel Growth Factor Reduced (GFR) (GFR) Matrix (Corning, USA) according to the manufacturer's instructions before cell seeding. The ECs were resuspended in the BMM-derived conditioned medium and seeded in the pre-coated well. Two hours later, the tube formation was observed and photographed using a Leica DM IL LED microscope (Carl Zeiss, Germany). The numbers of junctions, segments, and branches, as well as the total length and branch length, were quantified using the ImageJ software (NIH, USA).

2.2.11. ALP and TRAP co-staining assay

The effects of the BMM-derived conditioned medium on regulating the balance between the osteogenesis and the osteoclastogenesis were evaluated by ALP and TRAP co-staining assay. The whole bone marrow cells isolated from long bones of mice (including both BMMs and MSCs) were seeded in 24-well plates at a density of $5 \times 10^4/\text{cm}^2$ and kept overnight for attachment. The cells were then treated with different BMM-derived conditioned mediums for 3 days. After the stimulation, the cells were fixed with 4% paraformaldehyde for 10 min and washed thoroughly with PBS. The cells were first incubated with the 1-Step NBT/BCIP substrate solution (ThermoFisher, USA) for 15 min in the dark and then incubated with the TRAP staining solution for 15 min at 60 °C. The nuclei of the cells were countered stained by methyl green (Sigma-Aldrich, USA). The microscopic images were captured under a Color Imaging Microscope (Carl Zeiss, Germany). The ALP positive area or the TRAP positive area was quantified using the ImageJ software (NIH, USA).

2.3. Statistical analysis

All data analyses were performed and illustrated using the Prism software (version 7, GraphPad, USA). The results were expressed as means \pm standard error of the mean (SEM). The exact sample size (n) for each experimental group was clearly shown as dot plots in the figures and indicated in the legends. For comparisons among multiple groups, a one-way or a two-way analysis of variance (ANOVA) was used, followed by Tukey's multiple-comparison *post hoc* test. The levels of significant difference among the groups were defined and noted as *P < 0.05 and **P < 0.01. The sample size was decided based on preliminary data, as well as on observed effect sizes.

3. Results

3.1. Presence of TRAP + MNGCs at the early stage of new bone formation

To confirm the involvement of heterogeneous macrophage phenotypes, particularly the presence of MNGCs at the early stage of biomaterial-induced bone regeneration, we first analyzed the early tissue response when various metal ion-releasing bone biomaterials including magnesium implant, 3D-printed magnesium-containing polymer scaffold, porcine bone-derived biological apatite, zinc implant, and copper-bearing stainless steel, were implanted in rats.. Here, we observed a group of TRAP+ cells, either mononuclear or multinuclear, adjacent to the biomaterials implanted in the bone tissue on Day 7 (Fig. S1). Interestingly, unlike the classical TRAPhigh multinucleated osteoclast that commonly resides on the mineralized bone surface (magenta arrowhead, Figs. S1a-e), most of the TRAPlow/multinucleated cells (blue arrowhead, Figs. S1a-e) observed on Day 7 post-operation were not associated with matured bone. After confirming the presence of these multinucleated TRAP+ cells in our metal ionreleasing biomaterials, we concentrated on testing our hypothesis by using our well-established osteogenic biomaterials, namely Mg²⁺releasing alginate, in the rat model with the bone defect in the distal femoral region (Fig. S2). To further identify the presence of different phenotypes of macrophages, especially the biomaterial-related MNGCs, during the bone-healing course, we examined the sections over a series of time points after the injection of Mg²⁺-releasing alginate. On Day 3 after the operation, the defect was primarily filled with hematoma,

consisting mainly of erythrocytes trapped in a fibrinous network. The recruitment of immune cells and regenerative stem cells was only observed at the edge of the defect on Day 3, but their infiltration into the injured site became evident on Day 7 after the operation (Fig. 1a). Meanwhile, the hematoma observed in earlier periods had been replaced by a well-organized granulation tissue, rich in spindle-shaped cells. The corresponding TRAP staining images revealed that a group of TRAP⁺ cells, mostly mononuclear, located at the edge of the defect on Day 3, migrated to the periphery of the defect and became multinuclear on Day 7. On Day 14, the defect was occupied by newly formed bone; however, the bone structure in the defect remained primarily immature. Moreover, with the increase in the number of TRAP⁺ multinucleated cells on Day 14, more TRAP⁺ cells were found attached to either the bone surface or the blood vessels.

3.2. Characterization of functional phenotypes of macrophages during bone regeneration

Since we have identified Day 7 as the key time point for the infiltration of inflammatory macrophages into the defect, we particularly focus on the characterization of macrophage phenotypes at this stage. First, we used CD68 as the pan marker for resident macrophages (Fig. 1b) because the majority of inflammatory macrophages, MNGCs, and osteoclasts are generally derived from these common macrophage progenitors [30]. Next, we used another osteoclast marker, TRAP, to differentiate between MNGCs and osteoclasts. It was then interesting to find that there remained a considerable number of MNGCs with low or

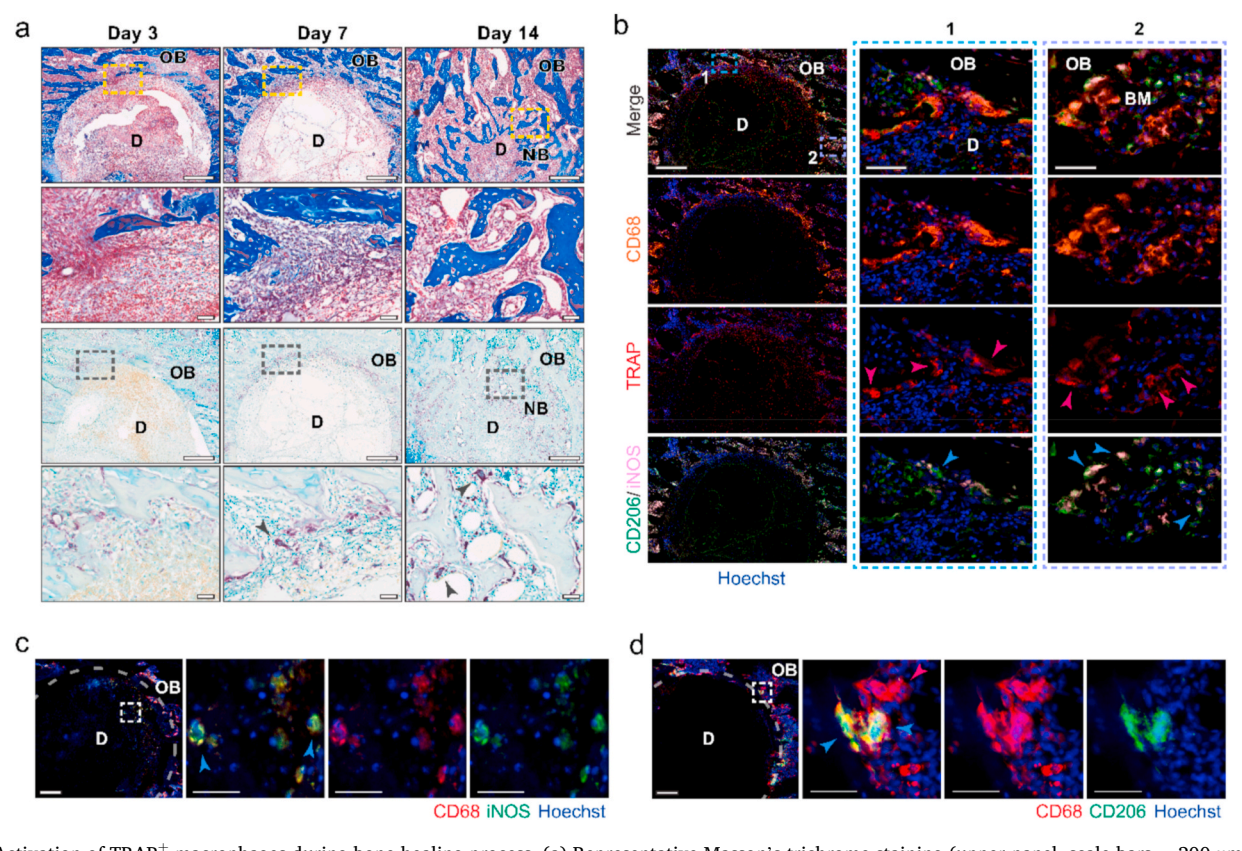


Fig. 1. Activation of $TRAP^+$ macrophages during bone-healing process. (a) Representative Masson's trichrome staining (upper panel, scale bars = $200 \mu m$) images and TRAP staining (lower panel, scale bars = $200 \mu m$) showing the new bone formation and the presence of $TRAP^+$ cells on Days 3, 7, and 14 after the delivery of Mg^{2+} -releasing alginate in the femoral defect (n = 3). High-magnification of the boxed regions (scale bars = $40 \mu m$) are shown. (b) Representative multicolor IHC image for CD68, TRAP, CD206, and iNOS showing the phenotypes of macrophages located at the periphery of the femoral defect on Day 7 (n = 3). Tile scans (scale bars = $400 \mu m$) and high magnification of the boxed regions (scale bars = $100 \mu m$) are shown. (c, d) Representative immunofluorescent images showing the presence of iNOS⁺ mononuclear macrophages (c) and CD206⁺ multinuclear macrophages (d) on Day 7 of bone healing (n = 4). Tile scans (scale bars = $200 \mu m$) and high magnification of the boxed regions (scale bars = $50 \mu m$) are shown. (OB: old bone; D: defect; NB: new bone; BM: bone marrow; pink arrowhead: $TRAP^+$ MNGC; blue arrowhead: $TRAP^+$ MNGC). (For interpretation of the references to color in this figure legend, the reader is referred to the Web version of this article.)

even no TRAP expression. Instead, they were identified as positive in CD206. Besides, the majority of CD68⁺iNOS⁺ macrophages were found to be mononucleated. With respect to the localization of different phenotypes of macrophages, most of the CD68⁺ macrophages observed in the defect area were mononuclear and positive in iNOS (Fig. 1c). In contrast, CD206⁺ macrophages, either mononucleated or multinucleated, appeared to be primarily located at the boundary of the defect, close to but not necessarily attached to the bone surface (Fig. 1d).

We then adopted a multiplex IHC assay to visualize the migration of macrophages and the shift in their functional phenotypes in correlation with the osteogenic activity. On Day 3 after the injury, inflammatory macrophages were primarily found near the bone trabecula around the defect (Fig. 2a). More interestingly, these macrophages, especially the dominant iNOS⁺ ones, were in close contact with the Osterix⁺ boneforming cells by forming a canopy-like structure over these cells or by being directly intercalated among these active osteoblasts.

By Day 7 after the surgery, the infiltration of numerous inflammatory macrophages, including both iNOS $^+$ M1 macrophages and CD206 $^+$ M2 macrophages, was evident at the periphery of the defect (Fig. 2b). These macrophages were present throughout the newly formed woven bones around the border of the defect. The majority of these iNOS $^+$ or CD206 $^+$ macrophages were observed as interlaced with the matrix-osteoid deposited on the bone trabecula. Compared with the earlier time point, there were considerably more TRAP $^+$ multinucleated cells at the periphery of the defect on Day 7. However, unlike the iNOS $^+$ or CD206 $^+$

macrophages that were both shown to be intimately associated with active osteoblasts, TRAP⁺ multinucleated cells were rarely observed adjacent to Osterix⁺ bone-forming cells. While TRAP⁺ CD206⁻ osteoclasts were restricted to the surface of active bone-remodeling sites, characterized by resorption lacunae in the bone underneath these cells, TRAP^{low} CD206⁺ multinucleated cells were more frequently observed on the matrix-osteoid-bone surface of the newly formed bone.

By Day 14 after the surgery, with the prominent new bone formation in the defect, the inflammatory macrophages were found to be interlaced throughout the newly formed bone trabecula within the defect area (Fig. 2c). Moreover, with the gradual increase in the number of CD206⁺ M2 macrophages and the marked decrease in the number of iNOS⁺ M1 macrophages, the dominant macrophage phenotype in the bone tissue microenvironment had been greatly altered. Moreover, the formation of woven bone trabecula and large blood vessels in the defect was accompanied by the presence of a considerable number of TRAP⁺ multinucleated cells, including both large TRAP⁺ CD206⁻ osteoclasts and TRAP^{low} CD206⁺ MNGCs.

On Day 56 after the operation, the defect had been filled with mineralized bone, and normal bone marrow tissue had also invaded the channel within the bone trabecula (Fig. 2d). It is interesting to find that at this late stage of bone healing, there remained a large number of $TRAP^{low}\,CD206^+$ or $TRAP^-\,CD206^+$ macrophages throughout the defect area.

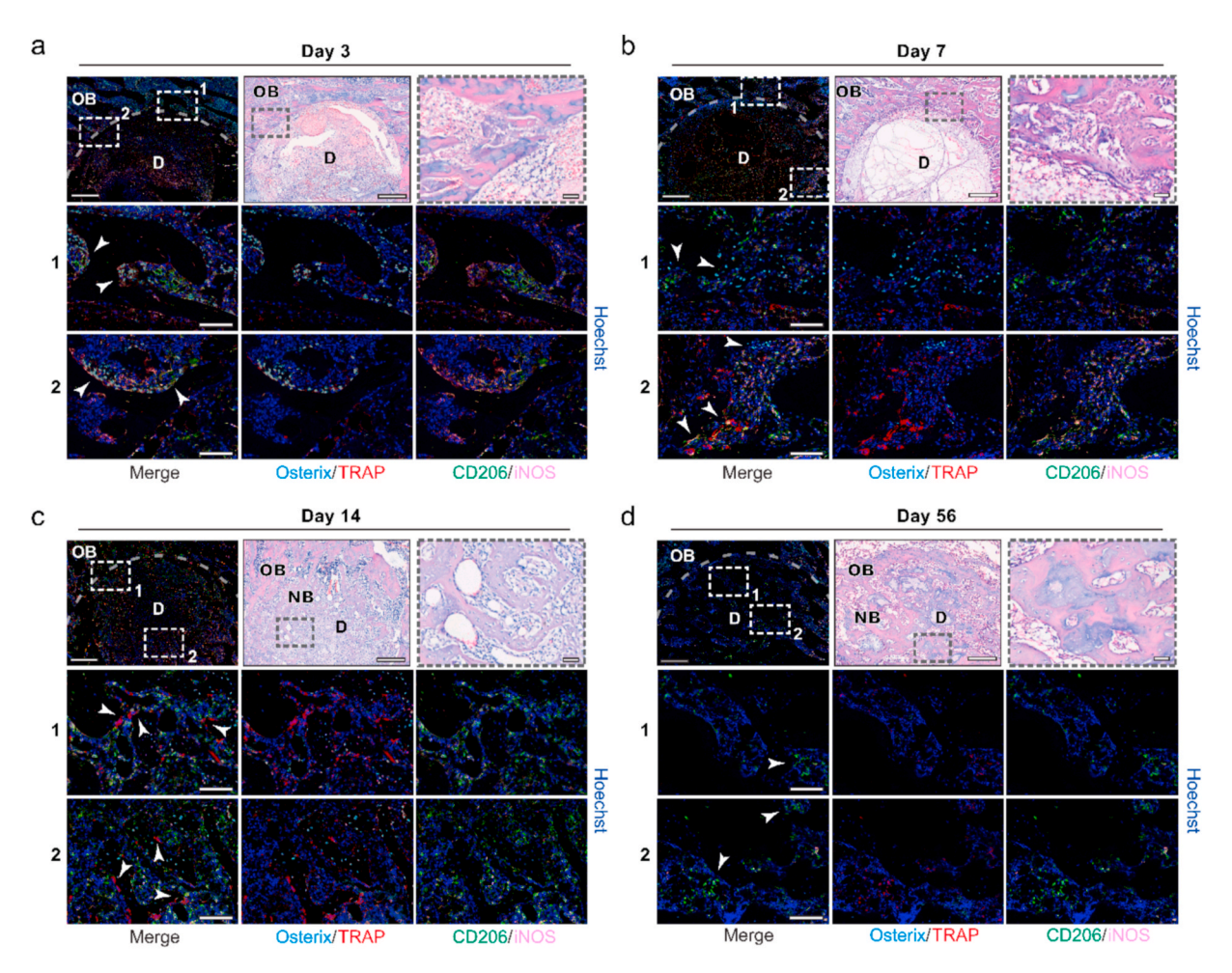


Fig. 2. Shifting of macrophage phenotypes during bone-healing process. (a–d) Representative multicolor IHC image for Osterix, TRAP, CD206, and iNOS showing the phenotypes of macrophages on Day 3 (a), Day 7 (b), Day 14 (c), and Day 56 (d) after the injection of alginate in the femoral defect (n = 3). Tile scans (scale bars = $400 \mu m$) and high magnification of the boxed regions (scale bars = $80 \mu m$) are shown. Corresponding H&E staining images (scale bars = $200 \mu m$) and high magnification of the boxed regions (scale bars = $40 \mu m$) are shown for better visualization of bone morphology in the grafted area. The representative macrophage phenotypes at each stage were indicated by white arrowhead.

3.3. The depletion of phagocytic macrophages impaired bone maturation

To support our findings that different macrophage phenotypes sequentially contributed to the whole course of bone healing, we analyzed the bone regeneration outcome in the liposomal clodronatetreated rats compared with the control group (Fig. 3a). The depletion of phagocytic macrophages at the early stage of the bone-healing process abolished the effect of Mg²⁺-releasing alginate on inducing new bone formation in the injured area (Fig. 3b and c). Serial μ CT scan from Day 3 to Day 56 after the surgery indicated that despite the notable increase in the BMD of the femoral defect in the liposomal clodronate-treated rats from Day 14 to Day 21, the loss of phagocytic macrophages led to the failure in the maintenance of newly formed bone structure at the boneremodeling stage. In turn, this resulted in significantly lower bone volume and density on Day 56 after the surgery compared with the control group. We then sought to confirm this finding by using histology data. As expected, after the injection of liposomal clodronate, either the TRAP⁺ multinucleated cells or the CD68⁺ multinucleated cells were completely depleted on Day 7 after the surgery (Fig. 3d). However, it was noteworthy that a small number of TRAP+ mononuclear cells and CD68+ mononuclear cells were still scattered throughout the newly formed woven bone in the defect. It was even more interesting to find that though the defect had been filled with immature woven bone, most of the bone trabecula disappeared after the bone-remodeling stage, leaving very few mineralized bones within the defect area by Day 56 after the surgery (Fig. 3e).

3.4. Fusion and multinucleation of macrophages

To gain a better understanding of the cellular functions of different phenotypes of multinucleated macrophages observed *in vivo*, we isolated primary BMMs from the long bones of mice and polarized them *in vitro* (Fig. 4a). We showed that both the classical M2 macrophage induction

medium (i.e., IL-4 + IL-13) and the osteoclast differentiation medium (i. e., M-CSF + RANKL) contributed to the fusion of BMMs and the upregulation of TRAP activity after the 6-day treatment. However, the classical M1 macrophage induction medium (i.e., LPS + IFN- γ) failed to induce more multinucleated or TRAP⁺ cells than in the control group, where no differentiation supplement was added (Fig. 4b and c). Moreover, the fusion rate and the number of multinucleated cells in BMMs treated with the osteoclast induction medium were twice than of BMMs treated with the M2 macrophage induction medium. Nevertheless, there was no significant difference between the two treatments in terms of the TRAP⁺ cells' rate. Furthermore, even if extending the induction time using M-CSF and RANKL could lead to MNGCs with more nuclei (Fig. S3), the number of nuclei in multinucleated cells (defined as cells with more than three nuclei) remained similar on Day 6 after treatment.

We then verified the functional phenotypes of the multinucleated cells by RT-qPCR (Fig. 5a). Compared with the control group, the M1 induction medium only contributed to a slight upregulation (~two-fold) in the calcitonin receptor gene (CALCR) but rarely altered the expression of the cathepsin K gene (CTSK), the tartrate-resistant acid phosphatase gene (TRAP), and the receptor activator of nuclear factor kB gene (RANK). Meanwhile, the M2 induction medium led to a four-fold increase in the CTSK expression and more than a 12-fold increase in the TRAP expression. However, the M1 and the M2 groups had no significant difference in the expression of CALCR or RANK. The addition of osteoclast induction medium greatly upregulated all osteoclastogenesisrelated gene markers, including an approximately 50-fold increase in CTSK, an approximately 400-fold increase in TRAP, an approximately 15-fold increase in CALCR, and more than a two-fold increase in RANK. Instead of activating osteoclastogenesis-related genes leading to cell fusion, we showed that the M2 induction medium contributed to a significant upregulation in the signal regulatory protein alpha gene ($SIRP\alpha$) and the programmed death-ligand 1 gene (PD-L1), which have both been shown to play important roles in cell recognition and membrane fusion

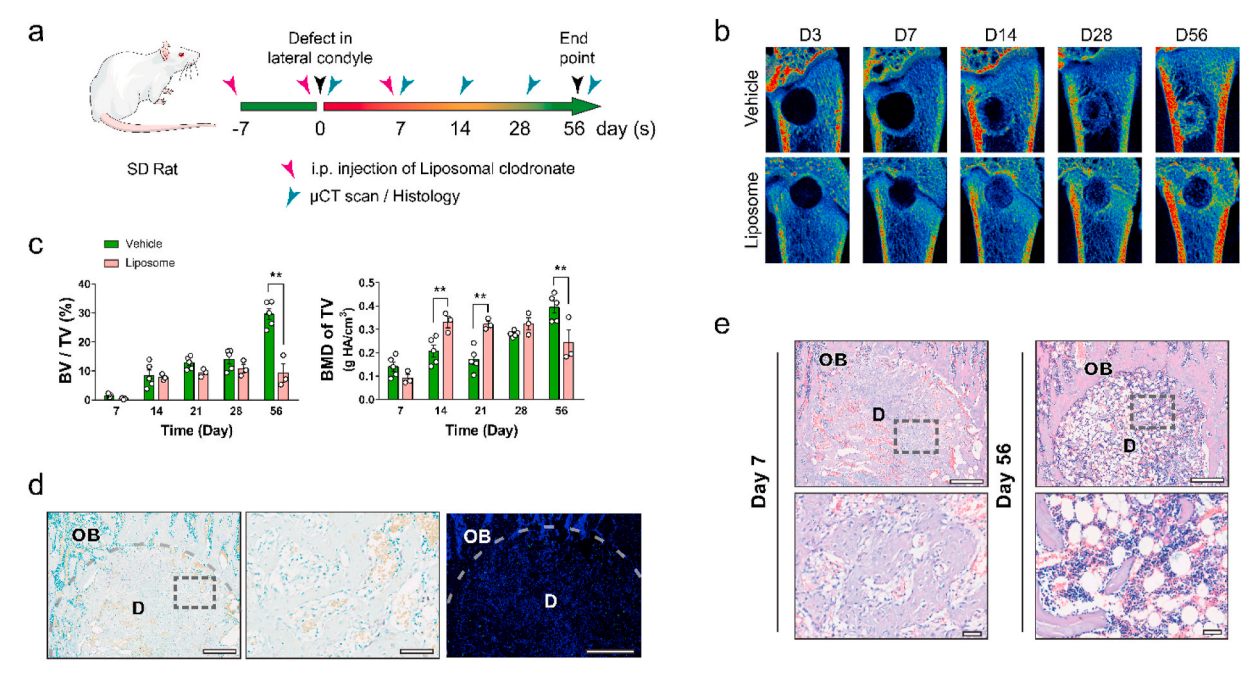


Fig. 3. Depletion of phagocytic macrophage impairs new bone formation. (a) Liposomal clodronate was administrated via intraperitoneal injection at the early stage of the bone-healing process for selective depletion of phagocytic macrophages. (b) Local bone mineral density heat mapping reconstruction using μ CT data showing the new bone formation in the femoral defect from Day 3 to Day 56 after the operation. (c) Corresponding quantification of trabecular bone fraction (BV/TV) and bone mineral density (BMD of TV) in the femoral defect. Data are presented as mean \pm standard error of the mean (SEM). **P < 0.01 by one-way ANOVA with Tukey's post hoc test. (d) Representative TRAP staining images (left scale bars = 200 μ m) and corresponding immunofluorescent images (right scale bars = 200 μ m) showing the depletion of TRAP+ cells or CD68+ cells in the femoral defect on Day 7 after the operation. High magnification of the boxed regions (scale bars = 40 μ m) is shown. (e) Representative H&E staining images (scale bars = 200 μ m) showing the formation of new bone in the femoral defect in phagocytic macrophage-depleted rat on Day 7 and Day 56 after the operation (n = 3). Lower images (scale bars = 40 μ m) show high magnification of the boxed regions.

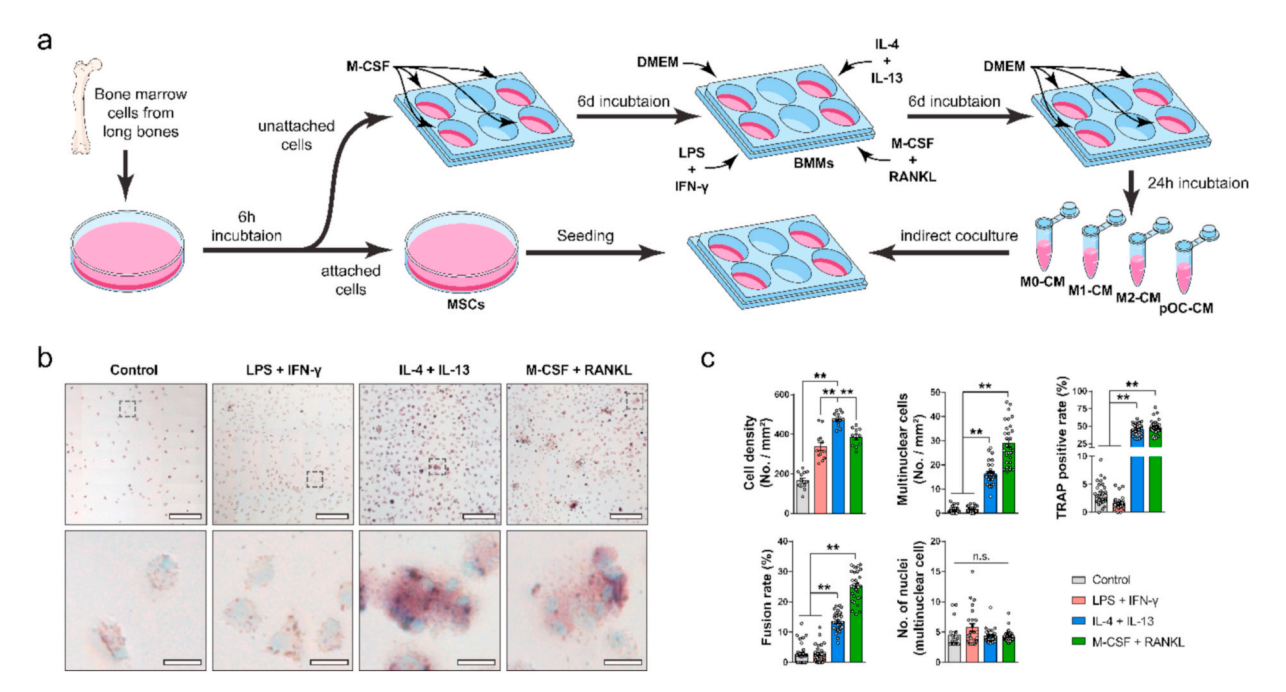


Fig. 4. TRAP activity and the fusion of macrophages using different induction strategies. (a) Schematic diagram showing the design of *in vitro* experiment. (b) Representative TRAP staining images (scale bars = $200 \ \mu m$) showing the formation of TRAP⁺ multinuclear macrophages after 6-day culture of mouse bone marrow-derived macrophages (BMMs) using M1 macrophage induction medium (LPS + IFN- γ), M2 macrophage induction medium (IL-4 + IL-13), and osteoclast induction medium (M-CSF + RANKL). High magnification of the boxed regions (scale bars = $20 \ \mu m$) is shown on the lower panel. (c) Corresponding quantification for cell density, number of multinuclear cells, TRAP⁺ cell rate, cell fusion rate, and the number of nuclei per multinuclear cell. Data are presented as mean \pm standard error of the mean (SEM). n.s. P > 0.05, **P < 0.01 by one-way ANOVA with Tukey's post hoc test.

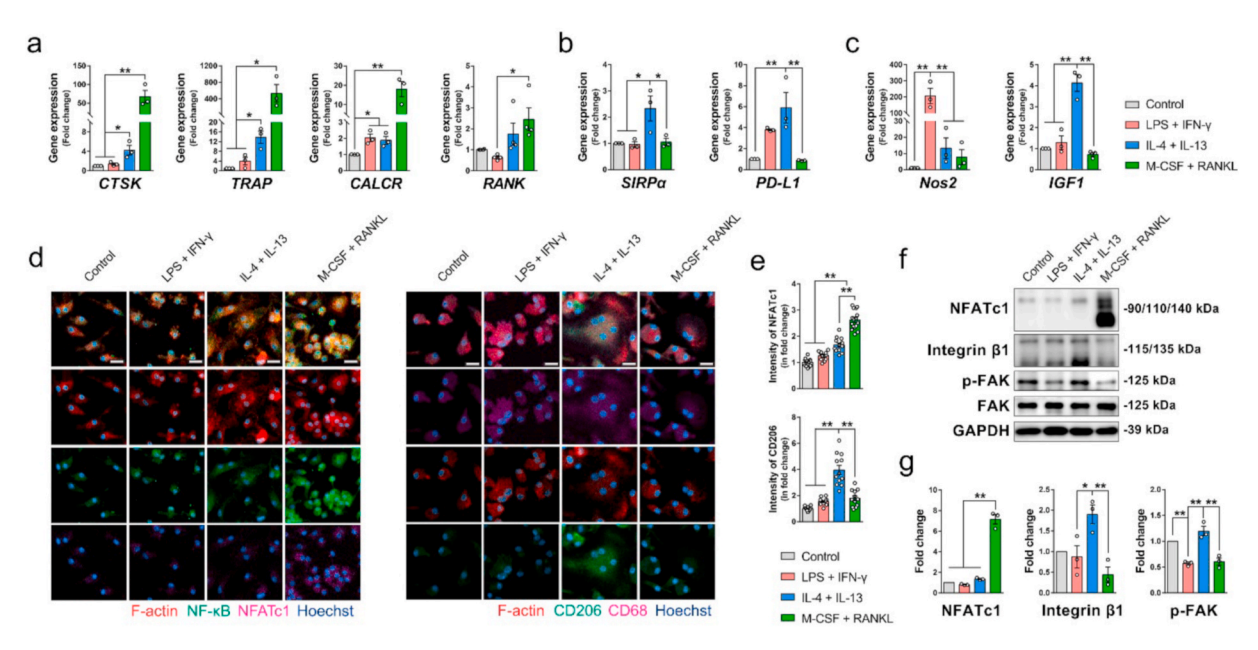


Fig. 5. Characterization of macrophage phenotype induced with different protocols. (a–c) The relative expression of osteoclastogenesis-related genes (a), cell fusion-related genes (b), and macrophage polarization marker genes (c) in BMMs after 6-day culture using different induction protocols. (d) Representative immunofluorescent images (scale bars = 50 μm) showing the cytoskeleton, as well as the expression of NF-κB, NFATc1, CD68, and CD206 in BMMs after 6-day culture using different induction protocols. (e) Corresponding quantification for relative fluorescent intensity of NFATc1 and CD206 in BMM. (f, g) Representative western blots (f) and corresponding quantification (g) showing the expression of NFATc1 and Integrin β1, as well as the phosphorylation of FAK in BMMs after 6-day culture using different induction protocols.

[31]. However, these genes were not altered by M1 or osteoclast induction (Fig. 5b). We also verified the differentiation of M1 and M2 macrophages by their respective marker genes, nitric oxide synthase 2 (*Nos2*) and insulin-like growth factor 1 (*IGF1*). While the M1 induction medium led to an almost 200-fold increase in the expression of *Nos2*, the

addition of the M2 induction supplement resulted in an approximately four-fold upregulation in the IGF1 expression (Fig. 5c).

Using immunocytochemistry, we showed that after the 6-day osteoclast induction, most of the fused cells were round in shape and had a diameter of approximately $50-100 \mu m$ (Fig. 5d). Meanwhile, there was a

significant increase in the expression of nuclear factor-kappa B (NF- κ B) and nuclear factor of activated T cells c1 (NFATc1), especially in the fused multinucleated cells (Fig. 5d and e). The shapes of the M2 induction medium-induced MNGCs showed a larger variety, ranging from round to polygon. Moreover, the expression of CD206 was significantly upregulated after the M2 induction (Fig. 5d and e). To confirm the distinct signaling mechanisms that osteoclasts and MNGCs adopted for cell fusion, we evaluated the key molecules involved in the cell fusion program using western blot assays. Our data demonstrated that only the osteoclast induction medium contributed to the increased expression of NFATc1 (Fig. 5f and g). In contrast, after the stimulation of IL-4 and IL-13, the upregulation in the expression of integrin β 1 and the phosphorylation of focal adhesion kinase (FAK) indicated that the formation of M2-like MNGCs might be mediated by signaling pathways distinct from osteoclasts.

3.5. Heterogeneous macrophage phenotypes led to a distinct immune microenvironment

As our data demonstrated the M2-like MNGC as a phenotype distinct from the classical activated M1-like macrophage or the pOC, we then compared the immunomodulatory functions of these macrophage phenotypes by studying the supernatant using the cytokine array and analyzing the gene expression using the RT-qPCR assay. Among the 111 tested cytokines and chemokines, we identified five factors (i.e., coagulation factor III, CCL2, IFN-7, IL-23, and Chemerin) significantly upregulated by M-CSF and RANKL but less altered by M2-like MNGCs (Fig. 6a). The cytokines/chemokines that were significantly upregulated in the secretome of M2-like MNGCs included CD160, complement component C5, chemokine (C-X3-C motif) ligand 1 (CX3CL1), Resistin, Periostin, E-selectin/CD62E, and RBP4. Although both pOC and M2-like MNGCs contributed to an approximately 1.5-2-fold increase in IL-22, there remained no significant difference between the two groups. Meanwhile, the M1 induction medium only led to an increased chemokine (C-C motif) ligand (CCL2) at a level comparable to that of the pOC group, as well as an increased complement component C5 and CX3CL1 equivalent to that of the M2 group.

To assess the immunomodulatory effects of the four phenotypes of macrophages, we further compared their expression patterns of inflammatory genes after the 6-day culture in the induction medium. In M2-like MNGCs, a series of inflammatory-related genes was upregulated

(Fig. 6b), including an approximately three-fold increase in CCL17 and interleukin-1 receptor antagonist (IL-1RA), as well as an approximately 1.5–2-fold increase in *IL-10*, transforming growth factor-beta 1 ($TGF\beta 1$), tumor necrosis factor-alpha (TNF-a), CX3CL1, and retinoic acid receptor responder protein 2 (RARRES2). The inflammatory-related genes that were most significantly upregulated by the M1 induction medium were CCL5, IL-6, vascular endothelial growth factor A (VEGFA), IL-1\(\beta\), oncostatin M (OSM), CCL2, C-X-C motif chemokine ligand 10 (CXCL10), IL-23, IL-22, CXCL1, CXCL2, and CD160 (Fig. 6c). It was noteworthy that the M2 induction medium also contributed to a nearly 30-fold increase in the expression of CCL5 and a two-fold increase in the expression of OSM compared with the control group (M0 macrophages); however, it was only at half of the level compared with the M1 group. Interestingly, regardless of the higher level of CCL2 in the secretome, the expression of the CCL2 gene was found to be significantly downregulated by the osteoclast induction medium. The M-CSF and the RANKL treatment also led to a 50% decline in the expression of IL-10 and TNF- α . Periostin (POSTN) remained to be the only tested gene that was significantly upregulated in the pOC group.

3.6. Effects of different phenotypes of macrophages on osteogenesis

Since our multiplex IHC data demonstrated that there remained some spatial relation between the macrophage lineage and the boneforming cells, we then investigated whether these macrophage phenotypes observed during the bone-healing processes contributed to osteogenic activities differently. Using confocal microscopy, we first showed that the migration of OCN+ osteoblasts to the injured site had been accompanied by the infiltration of CD68⁺ macrophages at the early stage (i.e., Day 7) of bone healing (Fig. 7a). This implied that the dominant phenotype of macrophage at this stage, which had been previously demonstrated to be M1 (Fig. 2b), could be closely associated with the recruitment of bone-forming cells. This hypothesis was verified by the cell proliferation assay (Fig. 7b) using primary CD29⁺, Sca-1⁺, and CD45 MSCs isolated from mouse long bones (Fig. S4). Our data demonstrated that the cell viability of MSCs cultured using the supernatant from M1 macrophages, M2-like MNGCs, and pOC was significantly higher than that of those treated with the supernatant from M0 macrophages (Fig. 7b). After the 7-day stimulation using the conditioned medium, the M1 macrophage led to a 30% increase in the cell viability of MSCs compared with the M0-CM group, while M2-CM or

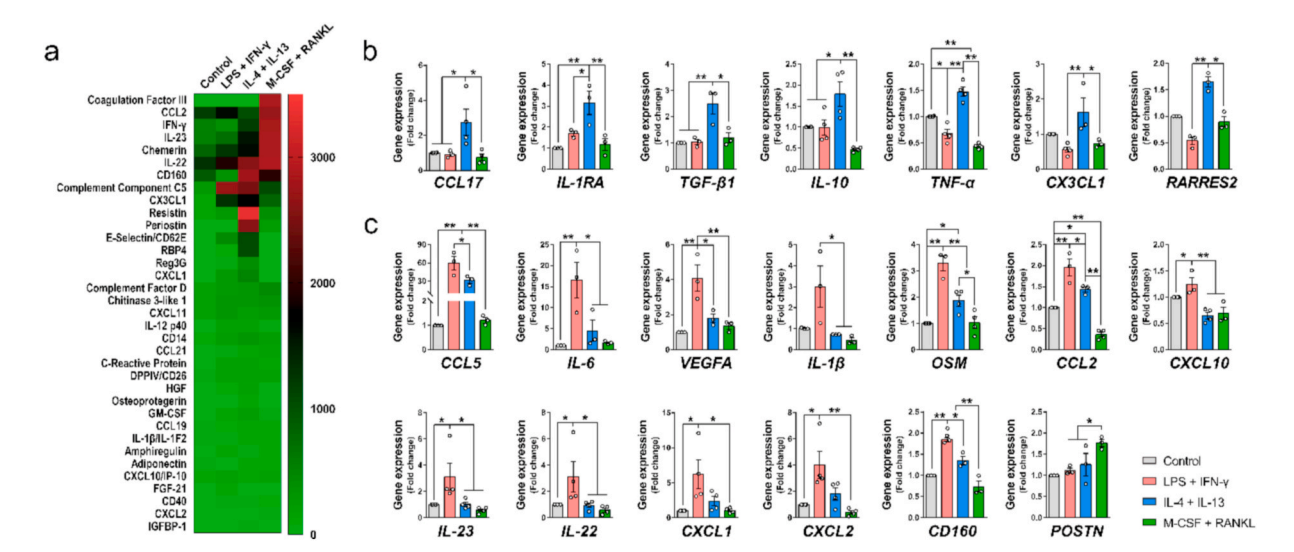


Fig. 6. The different polarization protocols for macrophages contribute to distinct inflammatory microenvironment. (a) Heat map of major inflammatory cytokines secreted from BMMs polarized using different induction strategies for 6 days. (b, c) The relative expression of inflammatory-related genes in BMMs after 6-day culture using different induction protocols. Data are presented as mean \pm standard error of the mean (SEM). *P < 0.05, **P < 0.01 by one-way ANOVA with Tukey's post hoc test.

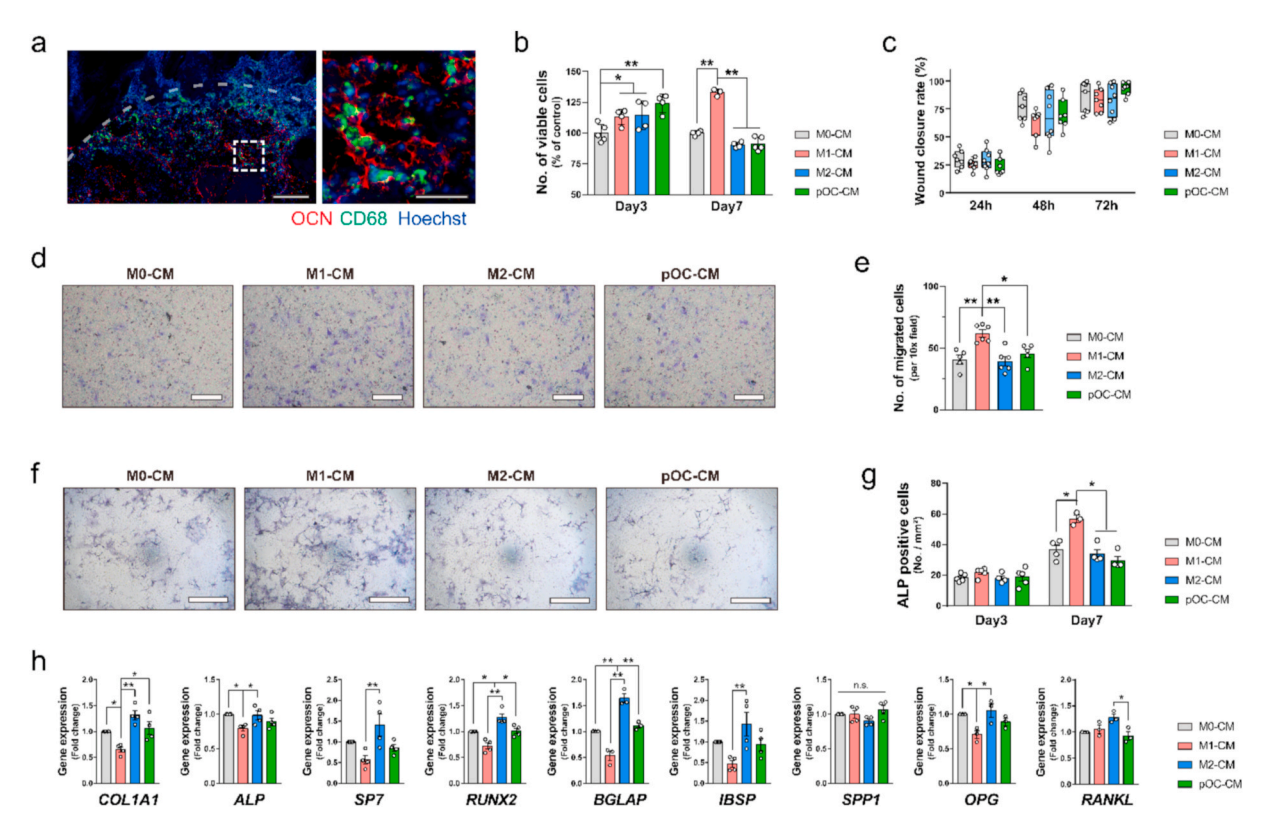


Fig. 7. The effects of different phenotypes of macrophages on osteogenesis. (a) Representative immunofluorescent images showing the colocalization of CD68⁺ macrophages and OCN⁺ osteoblasts in the femoral defect on Day 7 after the operation. Tile scans (scale bars = 200 μm) and high magnification of the boxed regions (scale bars = 50 μm) are shown. (b) Relative comparison of viable mesenchymal stem cell (MSC) cultured in conditioned medium from BMMs polarized using different induction protocols. (c) Wound closure rate of MSCs cultured in conditioned medium from BMMs polarized using different induction protocols. (d, e) Representative images (d, scale bars = 250 μm) and corresponding for quantification for the number of migrated MSCs in response to the stimulation of different BMM-derived conditioned medium. (f, g) Representative ALP staining images (f, scale bars = 500 μm) and corresponding quantification (g) for the number of ALP⁺ cells after 7-day culture in conditioned medium from BMMs polarized using different induction protocols. (h) The relative expression of osteogenesis-related and osteoclastogenesis-related genes in MSCs after 3-day culture in conditioned medium from BMMs polarized using different induction protocols. n.s. P > 0.05, *P < 0.05, *P < 0.05, *P < 0.01 by one-way ANOVA (e, h) or two-way ANOVA (b, c, g) with Tukey's post hoc test.

pOC-CM barely contributed to the proliferation of MSCs at this time point (Fig. 7b). Although our data using wound-healing assay suggested the secretome from various macrophage phenotypes has similar effect on the migration of MSCs (Fig. 7c, S5), further studies using transwell assay showed M1-CM was the strongest chemo-attractant among the four tested conditioned medium to induce the migration of MSCs (Fig. 7d and e).

Moreover, it was intriguing to find that only the conditioned medium from the M1 macrophage promoted the ALP activity of MSCs (Fig. 7f and g). Indeed, on Day 7 after the stimulation, M1-CM contributed to a 50% increase in the number of ALP⁺ MSCs compared with any other group. To confirm the effects of different macrophage phenotypes on osteogenic differentiation of MSCs, we further analyzed the expression of the osteogenic marker gene of MSCs after they were cultured in a macrophage conditioned medium (Fig. 7h). The conditioned medium from M2-MNGCs significantly promoted the genes related to the deposition and mineralization of the matrix, such as collagen type I alpha 1 (COL1A1), bone gamma-carboxyglutamate protein (BGLAP), and integrin binding sialoprotein (IBSP). In contrast, the M1 macrophage tended to suppress the three above-mentioned genes. The four groups had no significant difference in the expression of secreted phosphoprotein 1 (SPP1), which is also known to be involved in the mineralization of the extracellular matrix. Interestingly, the gene expression of ALP was shown to be slightly downregulated by M1-CM, in which the ALP activity of MSCs increased. Moreover, compared with the M1 macrophage, M2-MNGCs also contributed to the significantly increased expression of Sp7 transcription factor (SP7) and runt-related transcription factor 2 (*RUNX2*), which are both known to be vital for osteogenic differentiation of MSCs. In addition to the osteogenesis-related genes, M2-CM also led to a significantly higher level of osteoprotegerin (*OPG*) than M1-CM, while the difference in the expression of receptor activator of nuclear factor kappa-B ligand (*RANKL*) between the M1-CM and the M2-CM groups remained statistically insignificant. None of the tested genes was significantly altered by the conditioned medium from pOC when compared with the M0-CM group.

3.7. Effects of different phenotypes of macrophages on angiogenesis

In addition to the deposition of the bone matrix by the osteoblast lineage, angiogenesis also plays an important role in bone regeneration. We demonstrated that as the initial step of angiogenesis, the recruitment of CD31⁺ ECs occurred following the infiltration of CD68⁺ macrophages at an early stage (i.e., Day 7) of bone healing (Fig. 8a). Moreover, there seemed to be some spatial relation between the macrophages and the ECs, similar to what we previously observed between macrophages and the osteoblast lineage. We then compared the effects of the conditioned medium from different macrophage phenotypes on the proliferation and migration of primary ECs isolated from mouse aorta. On Day 3 after the stimulation, only M1-CM and pOC-CM led to a 10% increase in the cell viability of ECs compared with M0-CM (Fig. 8b). However, on Day 7, the conditioned medium from all of the three macrophage phenotypes (M1 $\,$ macrophage, M2-MNGCs, and pOC) was able to contribute to a 25-50% increase in the cell viability of ECs compared with the control group. Despite the effect on the proliferation, we found that M2-CM actually

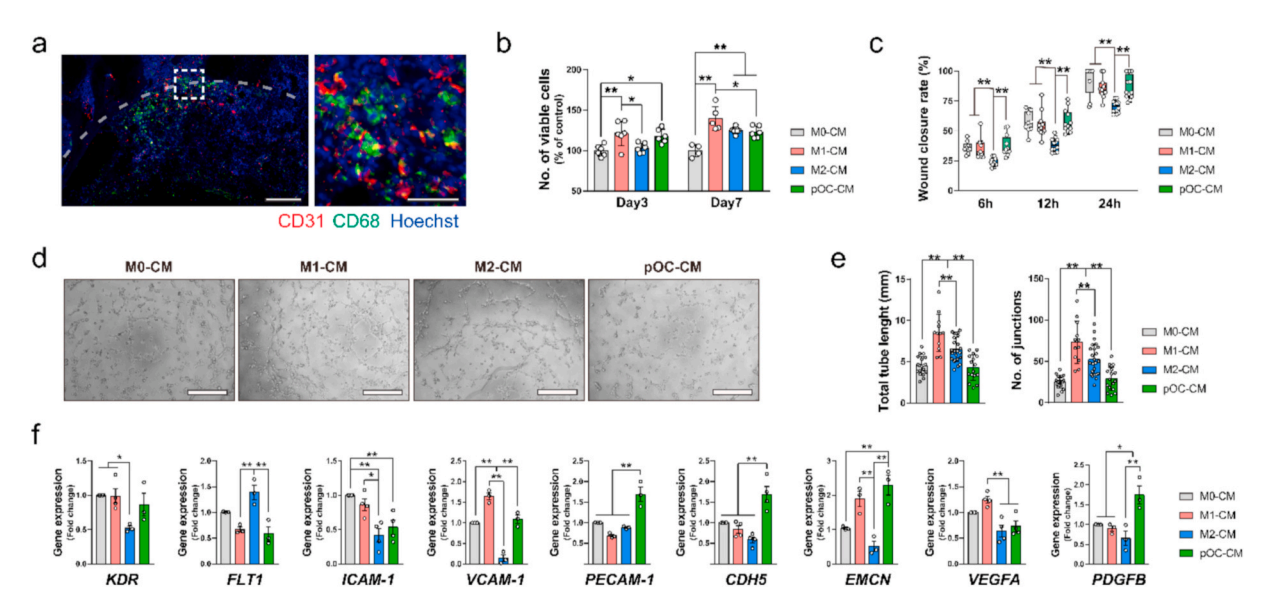


Fig. 8. The effects of different phenotypes of macrophages on angiogenesis. (a) Representative immunofluorescent images showing the colocalization of CD68⁺ macrophages and CD31⁺ endothelial cells in the femoral defect on Day 7 after the operation. Tile scans (scale bars = $200 \mu m$) and high magnification of the boxed regions (scale bars = $50 \mu m$) are shown. (b) Relative comparison of viable endothelial cells (ECs) cultured in conditioned medium from BMMs polarized using different induction protocols. (c) Wound closure rate of ECs cultured in conditioned medium from BMMs polarized using different induction protocols. (d, e) Representative images (d, scale bars = $500 \mu m$) and corresponding quantification (e) for tube formation of ECs on Matrigel after 2-h culture in conditioned medium from BMMs polarized using different induction protocols. (f) The relative expression of angiogenesis-related genes in ECs after 3-day culture in conditioned medium from BMMs polarized using different induction protocols. n.s. P > 0.05, *P < 0.05, *P

suppressed the migration of ECs in the wound-healing assay because the wound-healing rate in the M2-CM group had been lower than the other group throughout the assay (Fig. 8c, S6).

Next, we used tube formation assay, the most widely used in vitro assays to assess the differentiation of ECs into capillaries, in order to study the angiogenic potential of the conditioned medium from different macrophage phenotypes. M1-CM remained as the strongest stimulation for tube formation, as it contributed to the significantly increased total tube length and the number of junctions (Fig. 8d and e). Meanwhile, M2-CM was also more effective than M0-CM, but to a lesser extent than M1-CM, in inducing in vitro tube formation. Nevertheless, the conditioned medium from pOC failed to promote the tube formation further than M0-CM did. To further elucidate the effects of different immune microenvironments on the angiogenic differentiation of ECs, we analyzed a series of angiogenesis-related genes using RT-qPCR (Fig. 8f). Compared with the conditioned medium from the M0 macrophage, the M2-MNGCderived conditioned medium dramatically suppressed the expression of kinase insert domain receptor (KDR), which encodes the principal VEGF receptor, namely VEGFR2. The M2-CM also significantly downregulated the downstream of VEGF signaling, including intercellular adhesion molecule-1 (ICAM-1) and vascular cell adhesion molecule-1 (VCAM-1). In contrast, the conditioned medium from the M1 macrophage led to a 1.5-fold increase in the expression of VCAM-1 compared with the M0-CM group and an almost two-fold increase in the expression of VEGFA compared with either M2-MNGCs or pOC. More importantly, while the expression of KDR, ICAM-1, VCAM-1, and endomucin (EMCN) was significantly higher in M1-CM than in M2-CM, the expression of fmsrelated tyrosine kinase 1 (FLT1), which encodes VEGFR-1 that prevents the binding between VEGFA and VEGFR-2, was upregulated by more than 100% in the M2-CM group compared with that in the M1-CM group (Fig. 8f). Although pOC-CM decreased 50% of ICAM-1 expression as compared with that of M0-CM, the angiogenic marker genes, including platelet endothelial cell adhesion molecule (PECAM-1) and EMCN were found effectively upregulated. Moreover, pOC-CM was the only inflammatory stimuli to upregulate cadherin 5 (CDH5) and platelet derived growth factor subunit B (PDGFB).

3.8. Effects of different phenotypes of macrophages on osteoclastogenesis

Osteoclasts have been known to play an indispensable role in bone regeneration, especially at the remodeling stage. Besides the effects on osteogenesis and angiogenesis, we also evaluated the osteoclastogenic activity of BMMs varied by the different immune microenvironments induced by various macrophage phenotypes. We showed that in addition to the strong effect on upregulating the ALP activity of MSCs, M1-CM was also very effective in inducing osteoclast formation (Fig. 9a, b, 9c). Indeed, the M1 macrophage-derived conditioned medium after 3day stimulation resulted in the highest number of ALP⁺ osteoblasts among the four tested groups and significantly more TRAP⁺ multinucleated osteoclasts than in the M2-CM group. Using the RT-qPCR assay, we found that the expression of colony stimulating factor 1 (CSF1) was significantly downregulated by M1-CM but upregulated by M2-CM (Fig. 9d). Moreover, M1-CM led to around 1.5-fold increase in the expression of CALCR and CTSK, as well as a two-fold increase in the expression of TRAP compared with the other groups. Last but not least, the expression of RANK in the M2-CM group was only half of that in the M1-CM group.

4. Discussion

Over the years, the immune cells have been recognized to play vast and substantial roles in bone biology [32,33]. Given the high plasticity of the macrophage lineage in response to environmental cues and their fundamental role in regulating bone homeostasis, the macrophage dominant innate immune response is found to be the most critical factor determining the clinical outcome of bone regeneration [34,35]. In this study, we have shown that in an optimal bone-healing course, the desired biomaterial should be able to sequentially activate a series of macrophage phenotypes, from the initial pro-inflammatory M1 macrophage to the subsequent mononucleated and multinucleated pro-healing M2 macrophage, as well as the reparative osteoclasts (Fig. 9e). In particular, we have shown that there is no generally "good" or "bad" macrophage during bone healing. Instead, the shift in the dominant

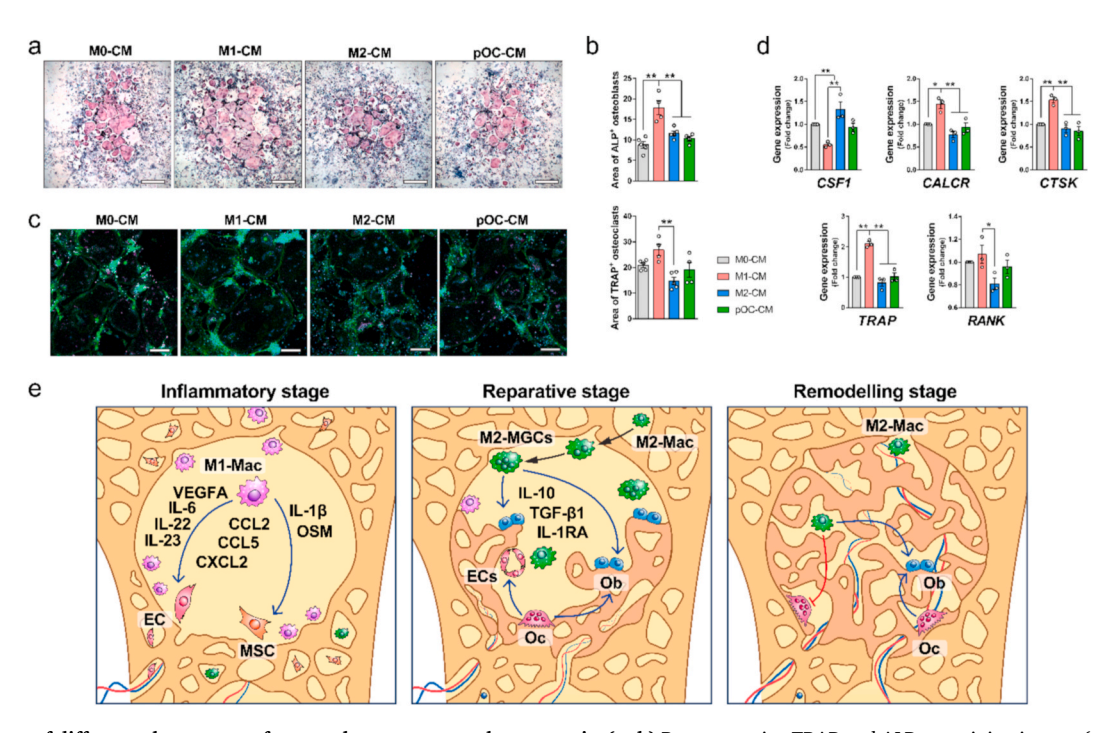


Fig. 9. The effects of different phenotypes of macrophages on osteoclastogenesis. (a, b) Representative TRAP and ALP co-staining images (a, scale bars = $200 \mu m$) and corresponding quantification (b) for the number of ALP⁺ cells and the number of TRAP⁺ cells after 3-day coculture of BMMs and MSCs using conditioned medium from BMMs polarized using different induction protocols. (c) Representative immunofluorescent images (scale bars = $100 \mu m$) showing the presence of actin rings in osteoclasts induced with conditioned medium from different phenotypes of macrophages. (d) The relative expression of osteoclastogenesis-related genes after 3-day coculture of BMMs and MSCs in conditioned medium from BMMs polarized using different induction protocols. Data are presented as mean \pm standard error of the mean (SEM). *P < 0.05 and *P < 0.01 by one-way ANOVA with Tukey's post hoc test. (e) The schematic diagram showing the shifting of macrophage phenotypes and their biological function during the bone-healing process.

macrophage phenotype in the injured site serves as a mechanism through which the immune system communicates with the skeletal system. Consequently, the recruitment, proliferation, differentiation, and cellular functions of multiple regenerative progenitor cells are tightly controlled by several waves of cytokines/chemokines stormed throughout the bone-healing course.

4.1. Indispensable role of M1 macrophages in initiating bone regeneration

The traditional notion of M1 macrophages was formed based on their role in the production of effector molecules (reactive oxygen species and nitric oxide) and inflammatory cytokines (IL-1 β , TNF- α , and IL-6) to combat bacterial and viral infections, as macrophages have been known to be the immune sentinels on the frontline of immune defense [36]. However, this notion of M1 macrophages might be misleading, especially in the field of tissue regeneration. In addition to their classical role in the elimination of pathogens, the critical roles of these pro-inflammatory macrophages in osteogenesis [37,38] and angiogenesis [39,40] at the early stage of bone regeneration have been gradually appreciated in recent years. Indeed, the depletion of macrophages at the early stage of fracture, which are primarily M1 macrophages rather than the other macrophage phenotypes, has been suggested as causing a more detrimental influence on new bone formation [41,42]. In our study, we confirmed the iNOS⁺ M1 macrophages to be the first wave of macrophages present in the femoral defect. We further demonstrated that M1 macrophages gave rise to the recruitment of osteoblasts to the injured site and were intimately associated with them on the surface of newly formed bone (Fig. 2a).

Meanwhile, our *in vitro* data showed that M1 macrophages induced by LPS and IFN- γ turned out to be the macrophage phenotype contributing to the proliferation of MSCs and ECs. Moreover, the conditioned medium from M1 macrophages was the most effective in promoting the ALP activity of MSCs while inducing the EC-derived capillary structure.

This is not surprising, given that M1 macrophages are the most efficient producers of inflammatory cytokines/chemokines, many of which have been demonstrated to contribute to the accumulation and differentiation of regenerative progenitor cells. For example, CCL2 and CCL5, two well-known chemokines responsible for the recruitment of immune cells at the inflammatory stage, have been shown to play key roles in bone healing by serving as chemoattractants for MSCs [43,44]. Additionally, several traditionally recognized pro-inflammatory cytokines that are primarily detected at the early stage of bone injury, including IL-6 [45], IL-1 β [46], and OSM [37,47], have been suggested as essential for bone healing. Last but not least, we found that M1 macrophages significantly enhanced the production of multiple inflammatory cytokines favoring angiogenesis, such as VEGFA [48], IL-22 [49], and IL-23 [50]. Therefore, adequate activation of M1 macrophages in response to bone biomaterials is necessary for initiating the bone-healing process.

However, it is worth noting that the regulatory effects for the majority of M1 macrophage-derived inflammatory chemokines/cytokines are time-dependent, as prolonged exposure to these pro-inflammatory factors, such as IL-1\beta and IL-6, leads to enhanced osteoclastogenesis [9]. We demonstrated that M1-CM strongly induced the formation of osteoclasts and significantly upregulated the expression of osteoclastogenesis-related genes, such as CALCR, CTSK, and TRAP (Fig. 9a and d). Moreover, compared with M1-CM, M2-CM not only promoted the expression of SP7 and RUNX2, leading to the osteogenic lineage commitment of stem cells [51], but also upregulated the expression of COL1A1, BGLAP, and IBSP, which are involved in the deposition and mineralization of the extracellular matrix [52]. Therefore, the switch from the initial pro-inflammatory M1 macrophage to the anti-inflammatory M2 phenotype is an important milestone in the bone-healing process [9]. Nevertheless, it is unlikely that these macrophage phenotypes are independent from each other and function separately. Instead, we have noticed that iNOS⁺ and CD206⁺ macrophages are closely associated with each other at the early stage of bone healing.

It was demonstrated that fully polarized M1 and M2 macrophages may reverse their polarization within 3 days [53]. Thus, there might exist a harmonic balance between M1 and M2 polarization and kinetics in their transition over time, according to the interaction between the host tissue and the local microenvironment near the biomaterial. In this context, the modulation of macrophage polarization could be a promising way to program the bone-healing process.

4.2. TRAP $^{\rm +}$ MNGCs can be M2 macrophages that contribute to bone regeneration

The fusion and multinucleation of macrophages can be classified into several morphological subtypes, depending on the arrangement and composition of their organelles, as well as their functional characteristics [54]. In skeletal tissues, the fusion of the monocyte-macrophage lineage is traditionally believed to lead to the formation of osteoclasts, which are characterized by their ability to resorb and replace bone grafts [16]. However, this point of view has been challenged by the identification of a group of MNGCs formed in response to the implantation of biomaterials. Despite a core fusion program existing in MNGCs and osteoclasts, the downstream pathways to induce fusion competency in these two multinucleated cells are distinct from each other [55]. In our study, we have demonstrated that in osteoclasts, RANKL signaling induces the expression of NFATc1, the master transcription factor for osteoclastogenesis [56]. In MNGCs, IL-4 and IL-13 contribute to the upregulation of integrin $\beta 1$ and integrin-mediated rearrangement of the cytoskeleton involving the phosphorylation of FAK [57]. As a result, the fusion-competent state is alternatively achieved by the activation of signal transducer and activator of transcription 6 (STAT6) [58,59].

Although there is no reliable marker to distinguish bone biomaterialrelated MNGCs from osteoclasts or other MNGCs in soft tissue in order to mediate pathogen clearance or chronic inflammation [10,55], the unique feature of M2-like MNGCs can be manifested by their different patterns of gene expression. First, only the stimulation of IL-4 and IL-13 leads to the upregulation of $SIRP\alpha$ and PD-L1, which are both critical in IL-4-induced macrophage fusion [60,61]. In contrast, the dramatically increased levels of CTSK, TRAP, and CALCR in osteoclasts compared with other macrophage phenotypes indicate that they are terminally differentiated cells for specialized cellular functions. Second, the MNGCs observed in the femoral defect in vivo and induced in vitro are clearly shown to uniquely express CD206, a widely used marker for M2 macrophage [4]. It is then not surprising to find that a variety of marker genes for M2 macrophages, including IGF1, IL-1RA, CCL17, TGFβ1, and IL-10 [62,63], are upregulated in MNGCs. This is consistent with the observation elsewhere that biomaterial-related MNGCs do not resorb bone but express M2 macrophage-like wound healing and inflammation-terminating molecules, such as Ym1, Arg1, and Alox15 [64]. Third, we have verified the biological functions of MNGC-derived secretome by indirect coculture. The conditioned medium from M2 MNGCs benefits the deposition and mineralization of the extracellular matrix by upregulating the expression of osteogenesis-related genes, in particular, COL1A1, BGLAP, and IBSP. This is similar to the finding on atherosclerosis progression, showing that a transient shift of M1 macrophages toward M2 MNGCs subsequently causes ectopic bone formation and calcification of arteries [65]. Therefore, it can be concluded that the accumulation of M2 MNGCs, which is considered pathological and potentially life-threatening elsewhere, can have significant therapeutic potential for bone regeneration in the microenvironment around the bone biomaterials.

Given the characteristics of M2 macrophages, some major differences exist between M2 MNGCs and mononuclear M2 macrophages. For instance, though more highly expressed in osteoclasts, some osteoclast marker genes (i.e., *TRAP*, *MMP9*, and *CTSK*) are found to be expressed in M2 MNGCs, as reported elsewhere [66,67]. Thus, these M2 MNGCs are found to be positive in TRAP staining, which has been extensively used for the identification of osteoclasts for decades [68]. In recent years,

increasing evidence shows that TRAP is not only expressed in osteoclasts and its progenitors but also activated in certain macrophages and dendritic cells [69]. Although previously, it has been debated whether there exists a special group of TRAP⁺ MNGCs in bone tissues other than osteoclasts [46,70], for the first time, we provide compelling evidence for the presence of TRAP⁺ M2 MNGCs during bone healing. More importantly, our data, combined with the results of various experiments over the past two decades [10], have clarified that MNGCs around orthopedic biomaterials differ from osteoclasts in terms of morphology, function, and behavior. The next interesting question would be whether the expression of osteoclast markers in MNGCs would indicate their tissue degradative properties or any unknown intracellular metabolic activity.

4.3. The participation of osteoclasts is essential for bone maturation

With the identification of new modes of cell-cell communication between osteoclasts and osteoblasts over the years, the central role of osteoclasts in bone homeostasis has been increasingly appreciated [17]. Compared with the inflammatory M1 and M2 macrophages, we have shown that osteoclasts participate in the bone-healing process at a later stage on Day 7 by residing on the newly formed woven bone. It is suggested that the provisional woven bone matrix, mainly deposited during the early stage of bone healing, should be subsequently resorbed by osteoclasts and replaced with lamellar bone at the bone-modeling and remodeling stage [20]. An elevation in the number of osteoclasts at the later stage of bone healing by the administration of M-CSF contributes to an increased area of mineralized callus [71]. In contrast, the inhibition of the osteoclast function via OPG [72], Denosumab [73], and Zoledronate [74] treatment results in compromised bone healing because osteoclast deficiency leads to a disorganized matrix and a reduced mineralization of bone structure [20]. In this study, we have shown that the depletion of the phagocytic macrophage lineage using liposomal clodronate (primarily targeting osteoclasts) contributes to abundant woven bone at the early stage of bone healing, resulting in higher BMD than the control group. However, this immature or primitive bone matrix can be quickly degraded at the remodeling stage by being unable to be properly mineralized, as it consists of interwoven coarse collagen fibers appearing as irregular bundles without preferential orientation [20]. Therefore, our results indicate that osteoclasts are not required for woven bone formation but are important during remodeling and consolidation of newly formed bone.

In addition to the regulation of bone remodeling, another fundamental role of osteoclasts during bone healing is the induction of angiogenesis. Suppression of osteoclast formation with OPG inhibits angiogenesis, while the administration of RANKL increases blood vessel density [75]. In our study, we have shown that unlike M1 macrophages that primarily contribute to the recruitment and angiogenic commitment of endothelial progenitor cells, the osteoclast lineage targets the functional maturation of the vascular structure, manifested by the upregulation of PECAM-1, CDH5, and EMCN genes [76]. Moreover, the osteoclast lineage is demonstrated to be the major source of PDGFB, which acts in a sequential fashion with VEGFA from M1 macrophages to stimulate and stabilize blood vessel growth [76,77]. Similar to osteoclasts, MNGCs have been extensively shown to be positively correlated with the vascularization of bone tissue [78,79]. Although the conditioned medium from M2 MNGCs induce a series of pro-angiogenesis cytokines, the M2-CM downregulates VEGFR-2 (the major receptor for VEGF signalling). In contrast, the M2-CM upregulates the VEGFR-1, which functions as an endothelial cell-intrinsic decoy receptor or ligand sink to negatively modulate VEGF signaling [80]. The controversy can be explained by a recent study using 3D tissue-engineered human blood vessel networks. Indeed, macrophages of distinct phenotypes differentially affect ECs behaviors. Although M1 macrophages initially enhance angiogenesis in vitro to a greater extent than the other macrophage phenotypes, M2 macrophages instead promote pericyte differentiation to support vessel stabilization and maturation [81].

Taken together, we have shown that the optimal angiogenesis process should include early stimulation from M1 macrophages and late support from M2 macrophages and osteoclasts.

5. Conclusion

In summary, our study demonstrates that the sequential activation of heterogeneous macrophage phenotypes is essential to achieve rapid bone healing without compromising peak bone density. The macrophage-osteoclast lineage, including M1 macrophages that dominate the acute inflammation stage and M2 macrophages that are present within the defect throughout the whole bone-healing course, as well as osteoclasts that join at the later remodeling stage, contribute to a highly orchestrated immune response in the microenvironment around the orthopedic biomaterials to control bone regeneration. Moreover, we have identified a group of TRAP+ MNGCs, frequently observed around bone biomaterials, as bearing the characteristics of M2 macrophages. Instead of mediating chronic inflammation or immune rejection, these M2 MNGCs turn out to be anti-inflammatory and favor tissue regeneration. The shift in macrophage phenotypes with interdispensable cellular functions during the bone-healing process suggests that the macrophage lineage can potentially serve as the mediator between the biomaterials and the bone tissue in order to facilitate accurate programming of the complex bone-healing process.

Author contributions

W. Qiao performed the animal surgery and conducted the histology study, as well as the *in vitro* and *in vivo* tests. H. Xie and J. Fang contributed to the isolation of primary cells and the cell culture, as well as the *in vitro* tests. J. Shen, W. Li, and D. Shen helped with the animal study and the data analysis. S. Wu, X. Liu, Y, Zheng, and K.M.C. Cheung helped with data analysis and interpretation. K.W.K. Yeung contributed to data interpretation and supervised the project. W. Qiao and K.W.K. Yeung wrote the manuscript, with input from all authors.

Data availability statement

The datasets generated during and/or analyzed during the current study are available from the corresponding author on reasonable request.

Declaration of competing interest

The authors declare that they have no known competing financial interests or personal relationships that could have appeared to influence the work reported in this paper.

Acknowledgments

We acknowledge HKU Li Ka Shing Faculty of Medicine, Faculty Core Facility for providing a harmonious work environment. This work is jointly supported by the National Key R&D Program, Ministry of Science and Technology of China (R&D#2018YFA0703100), the General Research Fund of Hong Kong Research Grant Council (Nos. 17207719, 17214516, and N_HKU725/16), the Hong Kong Health and Medical Research Fund (No.19180712), the Hong Kong Innovation Technology Fund (ITS/287/17 and ITS/405/18), Shenzhen Science and Technology Funding (JSGG20180507183242702), HKU-SZH Fund for Shenzhen Key Medical Discipline (SZXK2020084), and the Sanming Project of Medicine in Shenzhen, "Team of Excellence in Spinal Deformities and Spinal Degeneration" (SZSM201612055). The Science and Technology Commission of Shanghai Municipality (No. 18410760600), the International Partnership Program of Chinese Academy of Sciences (GJHZ1850), and the Guangdong Financial Fund for High-Caliber Hospital Construction (174-2018-XMZC-0001-03-2125/D-10).

Appendix A. Supplementary data

Supplementary data to this article can be found online at https://doi.org/10.1016/j.biomaterials.2021.121038.

References

- T.A. Einhorn, L.C. Gerstenfeld, Fracture healing: mechanisms and interventions, Nat. Rev. Rheumatol. 11 (1) (2015) 45–54.
- [2] K.A. Alexander, M.K. Chang, E.R. Maylin, T. Kohler, R. Muller, A.C. Wu, N. Van Rooijen, M.J. Sweet, D.A. Hume, L.J. Raggatt, A.R. Pettit, Osteal macrophages promote in vivo intramembranous bone healing in a mouse tibial injury model, J. Bone Miner. Res. 26 (7) (2011) 1517–1532.
- [3] Z. Chen, T. Klein, R.Z. Murray, R. Crawford, J. Chang, C. Wu, Y. Xiao, Osteoimmunomodulation for the development of advanced bone biomaterials, Mater. Today 19 (6) (2015) 304–321.
- [4] R.J. Miron, D.D. Bosshardt, OsteoMacs: key players around bone biomaterials, Biomaterials 82 (2016) 1–19.
- [5] M.K. Chang, L.J. Raggatt, K.A. Alexander, J.S. Kuliwaba, N.L. Fazzalari, K. Schroder, E.R. Maylin, V.M. Ripoll, D.A. Hume, A.R. Pettit, Osteal tissue macrophages are intercalated throughout human and mouse bone lining tissues and regulate osteoblast function in vitro and in vivo, J. Immunol. 181 (2) (2008) 1232–1244.
- [6] D. Yang, Y. Wan, Molecular determinants for the polarization of macrophage and osteoclast, Semin. Immunopathol. 41 (5) (2019) 551–563.
- [7] D.M. Mosser, J.P. Edwards, Exploring the full spectrum of macrophage activation, Nat. Rev. Immunol. 8 (12) (2008) 958–969.
- [8] C. Schlundt, T. El Khassawna, A. Serra, A. Dienelt, S. Wendler, H. Schell, N. van Rooijen, A. Radbruch, R. Lucius, S. Hartmann, G.N. Duda, K. Schmidt-Bleek, Macrophages in bone fracture healing: their essential role in endochondral ossification, Bone 106 (2018) 78–89.
- [9] L. Claes, S. Recknagel, A. Ignatius, Fracture healing under healthy and inflammatory conditions, Nat. Rev. Rheumatol. 8 (3) (2012) 133–143.
- [10] R.J. Miron, H. Zohdi, M. Fujioka-Kobayashi, D.D. Bosshardt, Giant cells around bone biomaterials: osteoclasts or multi-nucleated giant cells? Acta Biomater. 46 (2016) 15–28.
- [11] R. Milde, J. Ritter, G.A. Tennent, A. Loesch, F.O. Martinez, S. Gordon, M.B. Pepys, A. Verschoor, L. Helming, Multinucleated giant cells are specialized for complement-mediated phagocytosis and large target destruction, Cell Rep. 13 (9) (2015) 1937–1948.
- [12] S.S. Jensen, D.D. Bosshardt, R. Gruber, D. Buser, Long-term stability of contour augmentation in the esthetic zone: histologic and histomorphometric evaluation of 12 human biopsies 14 to 80 months after augmentation, J. Periodontol. 85 (11) (2014) 1549–1556.
- [13] B. ten Harkel, T. Schoenmaker, D.I. Picavet, N.L. Davison, T.J. de Vries, V. Everts, The foreign body giant cell cannot resorb bone, but dissolves hydroxyapatite like osteoclasts, PloS One 10 (10) (2015), e0139564.
- [14] J.L. Stockton, A.G. Torres, Multinucleated giant cell formation as a portal to chronic bacterial infections, Microorganisms 8 (11) (2020) 1637.
- [15] J.M. Anderson, A. Rodriguez, D.T. Chang, Foreign body reaction to biomaterials, Semin. Immunol. 20 (2) (2008) 86–100.
- [16] W.J. Boyle, W.S. Simonet, D.L. Lacey, Osteoclast differentiation and activation, Nature 423 (6937) (2003) 337–342.
- [17] X. Cao, Targeting osteoclast-osteoblast communication, Nat. Med. 17 (11) (2011) 1344–1346.
- [18] B. Gao, R. Deng, Y. Chai, H. Chen, B. Hu, X. Wang, S. Zhu, Y. Cao, S. Ni, M. Wan, L. Yang, Z. Luo, X. Cao, Macrophage-lineage TRAP+ cells recruit periosteumderived cells for periosteal osteogenesis and regeneration, J. Clin. Invest. 129 (6) (2019) 2578–2594.
- [19] R. Huang, X. Wang, Y.H. Zhou, Y. Xiao, RANKL-induced M1 macrophages are involved in bone formation, Bone Research 5 (2017) 1–13.
- [20] X.M. Dai, X.H. Zong, M.P. Akhter, E.R. Stanley, Osteoclast deficiency results in disorganized matrix, reduced mineralization, and abnormal osteoblast behavior in developing bone, J. Bone Miner. Res. 19 (9) (2004) 1441–1451.
- [21] A.L. Gamblin, M.A. Brennan, A. Renaud, H. Yagita, F. Lezot, D. Heymann, V. Trichet, P. Layrolle, Bone tissue formation with human mesenchymal stem cells and biphasic calcium phosphate ceramics: the local implication of osteoclasts and macrophages, Biomaterials 35 (36) (2014) 9660–9667.
- [22] W. Li, X. Liu, Y. Zheng, W. Wang, W. Qiao, K.W. Yeung, K.M. Cheung, S. Guan, O. B. Kulyasova, R. Valiev, In vitro and in vivo studies on ultrafine-grained biodegradable pure Mg, Mg–Ca alloy and Mg–Sr alloy processed by high-pressure torsion, Biomaterials Science 8 (18) (2020) 5071–5087.
- [23] J. Shen, W.H. Wang, X.Y. Zhai, B. Chen, W. Qiao, W. Li, P.H. Li, Y. Zhao, Y. Meng, S. Qian, X.Y. Liu, P.K. Chu, K.W.K. Yeung, 3D-printed nanocomposite scaffolds with tunable magnesium ionic microenvironment induce in situ bone tissue regeneration, Appl Mater Today 16 (2019) 493–507.
- [24] W. Qiao, R. Liu, Z. Li, X. Luo, B. Huang, Q. Liu, Z. Chen, J.K.H. Tsoi, Y.X. Su, K.M. C. Cheung, J.P. Matinlinna, K.W.K. Yeung, Z. Chen, Contribution of the in situ release of endogenous cations from xenograft bone driven by fluoride incorporation toward enhanced bone regeneration, Biomater Sci 6 (11) (2018) 2951–2964.
- [25] H.T. Yang, B. Jia, Z.C. Zhang, X.H. Qu, G.N. Li, W.J. Lin, D.H. Zhu, K.R. Dai, Y. F. Zheng, Alloying design of biodegradable zinc as promising bone implants for load-bearing applications, Nat. Commun. 11 (1) (2020) 1–16.

[26] L. Ren, H.M. Wong, C.H. Yan, K.W. Yeung, K. Yang, Osteogenic ability of Cubearing stainless steel, journal of biomedical materials Research, Part B, Applied Biomaterials 103 (7) (2015) 1433–1444.

- [27] H.M. Wong, K.W. Yeung, K.O. Lam, V. Tam, P.K. Chu, K.D. Luk, K.M. Cheung, A biodegradable polymer-based coating to control the performance of magnesium alloy orthopaedic implants, Biomaterials 31 (8) (2010) 2084–2096.
- [28] H.M. Wong, S. Wu, P.K. Chu, S.H. Cheng, K.D. Luk, K.M. Cheung, K.W. Yeung, Low-modulus Mg/PCL hybrid bone substitute for osteoporotic fracture fixation, Biomaterials 34 (29) (2013) 7016–7032.
- [29] J.M. Wang, A.F. Chen, K. Zhang, Isolation and primary culture of mouse aortic endothelial cells, JoVE 118 (2016), e52965.
- [30] J.W. Ashley, Z. Shi, H. Zhao, X. Li, R.A. Kesterson, X. Feng, Genetic ablation of CD68 results in mice with increased bone and dysfunctional osteoclasts, PloS One 6 (10) (2011), e25838.
- [31] J.C. Andrechak, L.J. Dooling, D.E. Discher, The macrophage checkpoint CD47: SIRPalpha for recognition of 'self' cells: from clinical trials of blocking antibodies to mechanobiological fundamentals, Philos. Trans. R. Soc. Lond. B Biol. Sci. 374 (1779) (2019) 20180217.
- [32] H. Takayanagi, Osteoimmunology: shared mechanisms and crosstalk between the immune and bone systems, Nat. Rev. Immunol. 7 (4) (2007) 292–304.
- [33] J. Lorenzo, M. Horowitz, Y. Choi, Osteoimmunology: interactions of the bone and immune system, Endocr. Rev. 29 (4) (2008) 403-440.
- [34] A.K. Gaharwar, I. Singh, A. Khademhosseini, Engineered biomaterials for in situ tissue regeneration, Nat Rev Mater 5 (9) (2020) 686–705.
- [35] C.M. Li, C.C. Guo, V. Fitzpatrick, A. Ibrahim, M.J. Zwierstra, P. Hanna, A. Lechtig, A. Nazarian, S.J. Lin, D.L. Kaplan, Design of biodegradable, implantable devices towards clinical translation, Nat Rev Mater 5 (1) (2020) 61–81.
- [36] P. Italiani, D. Boraschi, From monocytes to M1/M2 macrophages: phenotypical vs. functional differentiation, Front. Immunol. 5 (2014) 514.
- [37] P. Guihard, Y. Danger, B. Brounais, E. David, R. Brion, J. Delecrin, C.D. Richards, S. Chevalier, F. Redini, D. Heymann, H. Gascan, F. Blanchard, Induction of osteogenesis in mesenchymal stem cells by activated monocytes/macrophages depends on oncostatin M signaling, Stem Cell. 30 (4) (2012) 762–772.
- [38] O.M. Omar, C. Graneli, K. Ekstrom, C. Karlsson, A. Johansson, J. Lausmaa, C. L. Wexell, P. Thomsen, The stimulation of an osteogenic response by classical monocyte activation, Biomaterials 32 (32) (2011) 8190–8204.
- [39] E. Seebach, H. Freischmidt, J. Holschbach, J. Fellenberg, W. Richter, Mesenchymal stroma cells trigger early attraction of M1 macrophages and endothelial cells into fibrin hydrogels, stimulating long bone healing without long-term engraftment, Acta Biomater. 10 (11) (2014) 4730–4741.
- [40] K.L. Spiller, R.R. Anfang, K.J. Spiller, J. Ng, K.R. Nakazawa, J.W. Daulton, G. Vunjak-Novakovic, The role of macrophage phenotype in vascularization of tissue engineering scaffolds, Biomaterials 35 (15) (2014) 4477–4488.
- [41] L.J. Raggatt, M.E. Wullschleger, K.A. Alexander, A.C.K. Wu, S.M. Millard, S. Kaur, M.L. Maugham, L.S. Gregory, R. Steck, A.R. Pettit, Fracture healing via periosteal callus formation requires macrophages for both initiation and progression of early endochondral ossification, Am. J. Pathol. 184 (12) (2014) 3192–3204.
- [42] L. Vi, G.S. Baht, H. Whetstone, A. Ng, Q. Wei, R. Poon, S. Mylvaganam, M. Grynpas, B.A. Alman, Macrophages promote osteoblastic differentiation in-vivo: implications in fracture repair and bone homeostasis, J. Bone Miner. Res. 30 (6) (2015) 1090–1102.
- [43] L.C. Ortinau, H. Wang, K. Lei, L. Deveza, Y. Jeong, Y. Hara, I. Grafe, S.B. Rosenfeld, D. Lee, B. Lee, D.T. Scadden, D. Park, Identification of functionally distinct Mx1+ alphaSMA+ periosteal skeletal stem cells, Cell Stem Cell 25 (6) (2019) 784–796,
- [44] M. Ishikawa, H. Ito, T. Kitaori, K. Murata, H. Shibuya, M. Furu, H. Yoshitomi, T. Fujii, K. Yamamoto, S. Matsuda, MCP/CCR2 signaling is essential for recruitment of mesenchymal progenitor cells during the early phase of fracture healing, PloS One 9 (8) (2014), e104954.
- [45] X. Yang, B.F. Ricciardi, A. Hernandez-Soria, Y. Shi, N. Pleshko Camacho, M. P. Bostrom, Callus mineralization and maturation are delayed during fracture healing in interleukin-6 knockout mice, Bone 41 (6) (2007) 928–936.
- [46] M.L. Olmedo, P.S. Landry, K.K. Sadasivan, J.A. Albright, W.D. Meek, R. Routh, A. A. Marino, Regulation of osteoblast levels during bone healing, J. Orthop. Trauma 13 (5) (1999) 356–362.
- [47] P. Guihard, M.A. Boutet, B. Brounais-Le Royer, A.L. Gamblin, J. Amiaud, A. Renaud, M. Berreur, F. Redini, D. Heymann, P. Layrolle, F. Blanchard, Oncostatin m, an inflammatory cytokine produced by macrophages, supports intramembranous bone healing in a mouse model of tibia injury, Am. J. Pathol. 185 (3) (2015) 765–775.
- [48] J. Street, M. Bao, L. de Guzman, S. Bunting, F.V. Peale Jr., N. Ferrara, H. Steinmetz, J. Hoeffel, J.L. Cleland, A. Daugherty, N. van Bruggen, H.P. Redmond, R.A. Carano, E.H. Filvaroff, Vascular endothelial growth factor stimulates bone repair by promoting angiogenesis and bone turnover, Proc. Natl. Acad. Sci. U. S. A. 99 (15) (2002) 9656–9661.
- [49] N.J. Protopsaltis, W. Liang, E. Nudleman, N. Ferrara, Interleukin-22 promotes tumor angiogenesis, Angiogenesis 22 (2) (2019) 311–323.
- [50] C. Bridgewood, G.W. Fearnley, A. Berekmeri, P. Laws, T. Macleod, S. Ponnambalam, M. Stacey, A. Graham, M. Wittmann, IL-36 gamma is a strong inducer of IL-23 in psoriatic cells and activates angiogenesis, Front. Immunol. 9 (2018) 200.
- [51] T. Komori, Signaling networks in RUNX2-dependent bone development, J. Cell. Biochem. 112 (3) (2011) 750–755.
- [52] N.A. Twine, L. Chen, C.N. Pang, M.R. Wilkins, M. Kassem, Identification of differentiation-stage specific markers that define the ex vivo osteoblastic phenotype, Bone 67 (2014) 23–32.

[53] K.L. Spiller, S. Nassiri, C.E. Witherel, R.R. Anfang, J. Ng, K.R. Nakazawa, T. Yu, G. Vunjak-Novakovic, Sequential delivery of immunomodulatory cytokines to facilitate the M1-to-M2 transition of macrophages and enhance vascularization of bone scaffolds, Biomaterials 37 (2015) 194–207.

- [54] E.H. Chen, E.N. Olson, Unveiling the mechanisms of cell-cell fusion, Science 308 (5720) (2005) 369–373.
- [55] M. Pereira, E. Petretto, S. Gordon, J.H.D. Bassett, G.R. Williams, J. Behmoaras, Common signalling pathways in macrophage and osteoclast multinucleation, J. Cell Sci. 131 (11) (2018) jcs216267.
- [56] T. Negishi-Koga, H. Takayanagi, Ca2+-NFATc1 signaling is an essential axis of osteoclast differentiation, Immunol. Rev. 231 (2009) 241–256.
- [57] A.K. McNally, J.M. Anderson, Beta1 and beta2 integrins mediate adhesion during macrophage fusion and multinucleated foreign body giant cell formation, Am. J. Pathol. 160 (2) (2002) 621–630.
- [58] H. Miyamoto, E. Katsuyama, Y. Miyauchi, H. Hoshi, K. Miyamoto, Y. Sato, T. Kobayashi, R. Iwasaki, S. Yoshida, T. Mori, H. Kanagawa, A. Fujie, W. Hao, H. Morioka, M. Matsumoto, Y. Toyama, T. Miyamoto, An essential role for STAT6-STAT1 protein signaling in promoting macrophage cell-cell fusion, J. Biol. Chem. 287 (39) (2012) 32479–32484.
- [59] J.L. Moreno, I. Mikhailenko, M.M. Tondravi, A.D. Keegan, IL-4 promotes the formation of multinucleated giant cells from macrophage precursors by a STAT6dependent, homotypic mechanism: contribution of E-cadherin, J. Leukoc. Biol. 82 (6) (2007) 1542–1553.
- [60] N.P. Podolnikova, M. Hlavackova, Y.F. Wu, V.P. Yakubenko, J. Faust, A. Balabiyev, X. Wang, T.P. Ugarova, Interaction between the integrin Mac-1 and signal regulatory protein (SIRP) mediates fusion in heterologous cells, J. Biol. Chem. 294 (19) (2019) 7833–7849.
- [61] A.K. McNally, J.M. Anderson, Foreign body-type multinucleated giant cells induced by interleukin-4 express select lymphocyte co-stimulatory molecules and are phenotypically distinct from osteoclasts and dendritic cells, Exp Mol Pathol 91 (3) (2011) 673–681.
- [62] F.O. Martinez, S. Gordon, M. Locati, A. Mantovani, Transcriptional profiling of the human monocyte-to-macrophage differentiation and polarization: new molecules and patterns of gene expression, J. Immunol. 177 (10) (2006) 7303–7311.
- [63] O. Spadaro, C.D. Camell, L. Bosurgi, K.Y. Nguyen, Y.H. Youm, C.V. Rothlin, V. D. Dixit, IGF1 shapes macrophage activation in response to immunometabolic challenge, Cell Rep. 19 (2) (2017) 225–234.
- [64] E. Katsuyama, H. Miyamoto, T. Kobayashi, Y. Sato, W. Hao, H. Kanagawa, A. Fujie, T. Tando, R. Watanabe, M. Morita, K. Miyamoto, Y. Niki, H. Morioka, M. Matsumoto, Y. Toyama, T. Miyamoto, Interleukin-1 receptor-associated kinase-4 (IRAK4) promotes inflammatory osteolysis by activating osteoclasts and inhibiting formation of foreign body giant cells, J. Biol. Chem. 290 (2) (2015) 716–726.
- [65] J. Oh, A.E. Riek, S. Weng, M. Petty, D. Kim, M. Colonna, M. Cella, C. Bernal-Mizrachi, Endoplasmic reticulum stress controls M2 macrophage differentiation and foam cell formation, J. Biol. Chem. 287 (15) (2012) 11629–11641.
- [66] U.A. Khan, S.M. Hashimi, S. Khan, J. Quan, M.M. Bakr, M.R. Forwood, N. M. Morrison, Differential expression of chemokines, chemokine receptors and proteinases by foreign body giant cells (FBGCs) and osteoclasts, J. Cell. Biochem. 115 (7) (2014) 1290–1298
- [67] H. Kang, A. Kerloc'h, M. Rotival, X.Q. Xu, Q. Zhang, Z. D'Souza, M. Kim, J. C. Scholz, J.H. Ko, P.K. Srivastava, J.R. Genzen, W.G. Cui, T.J. Aitman, L. Game, J. E. Melvin, A. Hanidu, J. Dimock, J. Zheng, D. Souza, A.K. Behera, G. Nabozny, H. T. Cook, J.H.D. Bassett, G.R. Williams, J. Li, A. Vignery, E. Petretto, J. Behmoaras, Kcnn4 is a regulator of macrophage multinucleation in bone homeostasis and inflammatory disease, Cell Rep. 8 (4) (2014) 1210–1224.
- [68] M.S. Burstone, Histochemical demonstration of acid phosphatase activity in osteoclasts, J. Histochem. Cytochem. 7 (1) (1959) 39–41.
- [69] A.R. Hayman, Tartrate-resistant acid phosphatase (TRAP) and the osteoclast/ immune cell dichotomy, Autoimmunity 41 (3) (2008) 218–223.
- [70] J. Lorenz, A. Kubesch, T. Korzinskas, M. Barbeck, C. Landes, R.A. Sader, C. J. Kirkpatrick, S. Ghanaati, TRAP-positive multinucleated giant cells are foreign body giant cells rather than osteoclasts: results from a split-mouth study in humans, J. Oral Implantol. 41 (6) (2015) e257–e266.
- [71] K. Sarahrudi, M. Mousavi, K. Grossschmidt, N. Sela, F. Konig, V. Vecsei, S. Aharinejad, The impact of colony-stimulating factor-1 on fracture healing: an experimental study, J. Orthop. Res. 27 (1) (2009) 36–41.
- [72] M. Ulrich-Vinther, T.T. Andreassen, Osteoprotegerin treatment impairs remodeling and apparent material properties of callus tissue without influencing structural fracture strength, Calcif. Tissue Int. 76 (4) (2005) 280–286.
- [73] L.C. Gerstenfeld, D.J. Sacks, M. Pelis, Z.D. Mason, D.T. Graves, M. Barrero, M. S. Ominsky, P.J. Kostenuik, E.F. Morgan, T.A. Einhorn, Comparison of effects of the bisphosphonate alendronate versus the RANKL inhibitor denosumab on murine fracture healing, J. Bone Miner. Res. 24 (2) (2009) 196–208.
- [74] M.M. McDonald, S. Dulai, C. Godfrey, N. Amanat, T. Sztynda, D.G. Little, Bolus or weekly zoledronic acid administration does not delay endochondral fracture repair but weekly dosing enhances delays in hard callus remodeling, Bone 43 (4) (2008) 653-669
- [75] F.C. Cackowski, J.L. Anderson, K.D. Patrene, R.J. Choksi, S.D. Shapiro, J.J. Windle, H.C. Blair, G.D. Roodman, Osteoclasts are important for bone angiogenesis, Blood 115 (1) (2010) 140–149.
- [76] E.M. Conway, D. Collen, P. Carmeliet, Molecular mechanisms of blood vessel growth, Cardiovasc. Res. 49 (3) (2001) 507–521.
- [77] H. Xie, Z. Cui, L. Wang, Z. Xia, Y. Hu, L. Xian, C. Li, L. Xie, J. Crane, M. Wan, G. Zhen, Q. Bian, B. Yu, W. Chang, T. Qiu, M. Pickarski, L.T. Duong, J.J. Windle,

X. Luo, E. Liao, X. Cao, PDGF-BB secreted by preosteoclasts induces angiogenesis during coupling with osteogenesis, Nat. Med. 20 (11) (2014) 1270-1278.

- [78] S. Ghanaati, R.E. Unger, M.J. Webber, M. Barbeck, C. Orth, J.A. Kirkpatrick, P. Booms, A. Motta, C. Migliaresi, R.A. Sader, C.J. Kirkpatrick, Scaffold vascularization in vivo driven by primary human osteoblasts in concert with host inflammatory cells, Biomaterials 32 (32) (2011) 8150-8160.
 [79] M. Barbeck, S. Udeabor, J. Lorenz, M. Schlee, M.G. Holthaus, N. Raetscho,
- - J. Choukroun, R. Sader, C.J. Kirkpatrick, S. Ghanaati, High-temperature sintering
- of xenogeneic bone substitutes leads to increased multinucleated giant cell formation: in vivo and preliminary clinical results, J. Oral Implantol. 41 (5) (2015) e212–222.
- [80] B. Sivakumar, L.E. Harry, E.M. Paleolog, Modulating angiogenesis: more vs less, J. Am. Med. Assoc. 292 (8) (2004) 972–977.
- [81] P.L. Graney, S. Ben-Shaul, S. Landau, A. Bajpai, B. Singh, J. Eager, A. Cohen, S. Levenberg, K.L. Spiller, Macrophages of diverse phenotypes drive vascularization of engineered tissues, Sci Adv 6 (18) (2020), eaay6391.